Compatibilizer effectiveness for the reuse of mixed post-consumer solid waste plastic towards Distributed recycling additive manufacturing

Catalina Suescun Gonzalez, Benjamin Sandei, Fabio Cruz Sanchez, Sandrine Hoppe, Hakim Boudaoud, Joshua Pearce, Cécile Nouvel

Compatibilizer effectiveness for the reuse of mixed post-consumer solid waste plastic towards Distributed recycling additive manufacturing

Catalina Suescun Gonzalez [1,3,], Benjamin Sandei [3,4], Fabio A. Cruz Sanchez[1], Sandrine Hoppe[3], Hakim Boudaoud[1], Joshua M. Pearce[2], Cécile Nouvel[3]

[1]Université de Lorraine, ERPI, F-54000, Nancy, France.
[2]Department of Electrical & Computer Engineering and Ivey Business School, Western University, London, ON Canada
[3]Université de Lorraine, CNRS, LRGP, F-54000 Nancy, France
[4]INSA Lyon, CNRS UMR 5223, Ingénierie des Matériaux Polymères, F-69621Villeurbanne, France

Abstract

The concept of bypassing the sorting process in post-consumer plastic recycling has emerged as an intriguing solution to circumvent the high costs and inherent inefficiencies of conventional processes. This approach demands the blend of polymers, whose physical properties have been known to be improved with the use of compatibilizers. In this study, the recycled polymer blends based on the two largest-volume waste plastics of poly (ethylene terephthalate) (rPET) and high-density polyethylene (rHDPE) at 90/10 wt% are investigated to develop a method that would be able to recycled water bottles directly. This blend was investigated with and without 10 wt% of three types of styrene-ethylene/butylene (SEBS), two non-reactive compatibilizers named by their code G1650 and G1652 and one maleated SEBS cirKular+ c1010 – (C1010). It was prepared in a co-rotating twin screw extruder and 3-D printed using a large-format fused granular fabrication printer. The results showed that samples manufactured by conventional methods exhibited increases of approximately 50% in tensile strength and 34% in impact strength compared to those produced by 3D printing. Furthermore, the addition of compatibilizers enhanced the elongation at break by approximately 40% in samples processed through conventional methods.

Keywords: polymer blend, compatibilizer, fused granular fabrication, additive manufacturing, recycling.

List of Abbreviations

Acronym	Definition
ABS	Poly(acrylonitrile-co-butadiene-co-styrene)
DRAM	Distributed recycling and additive manufacturing
DSC	Differential Scanning Calorimetry
DTG	Derivative Thermogravimetric Analysis
E-AA	Polyethylene-co-acrylic acid
EPM	Ethylene-propylene
EPDM	ethylene-propylene-diene
FGF	Fused granular fabrication
FTIR	Fourier-Transform Infrared Spectroscopy
GMA	Glycidyl methacrylate

HDPE	High density polyethylene
HIPS	High impact polystyrene
LDPE	Low-density polyethylene
MA	Maleic anhydride
MDSC	Modulated differential scanning calorimetry
MEX	Material extrusion
MFI	Melt-Flow Index
PA	Polyamide
PC	Polycarbonate
PE	Polyethylene
PET	Polyethylene terephthalate
PP	Polypropylene
PS	Polystyrene
PSW	Plastic solid waste
rHDPE	Recycled high density polyethylene
rPET	Recycled polyethylene terephthalate
rPP	Recycled polypropylene
SB	Styrene-butadiene
SEBS	Poly(styrene-b-(ethylene-co-butylene)-b-styrene)
SEBS-g-MA	Maleic anhydride-grafted SEBS
SEM	Scanning Electron Microscopy
TGA	Thermogravimetric Analysis

1. Introduction

Plastics have become an indispensable material for a wide range of applications including: beverage packaging, construction, automotive, electrical and electronic equipment, due to their exceptional properties [1]. They offer advantages such as high mechanical strength, low density, lightweight nature, ease of processing, and cost-effectiveness [2]. Plastic solid waste (PSW), however, has emerged as a major source of contamination, causing environmental concerns [3]. The packaging industry is responsible for generating approximately 40% of the plastic waste [4]. Remarkably, polymers such as polyethylene (PE), polypropylene (PP), and poly(ethylene terephthalate) (PET) collectively comprise over 90% of all packaging, solidifying their position as the most common employed polymers within this sector [5]. Despite the predominance of recycling as the preferred method for plastic waste disposal, inadequate waste management has resulted in alarming poor statistics. In European countries, only 32.5% of plastic is recycled, 42.6% is incinerated for energy recovery, and 24.9% ends up in landfills, according to Plastics Europe [6]. The situation is even more concerning in other areas. For example, in India a staggering 80% of plastic waste is consigned to landfills, 8% is incinerated, and only 7% is recycled [7]. The challenges encountered in plastic recycling can be attributed to a shortage of collection infrastructure, the complexity of effectively sorting various plastic types, the high costs, and the time-consuming nature of collecting and processing plastic waste [6], [7].

In recent years, there has been a growing interest in recycling plastics without prior sorting as an appealing alternative to mitigate the associated cost [10]. One example of this trend is the initiative in Europe, which encourages keeping the bottle and cap together as part of the EU

Directive 2019/904 in the single-use plastic products [11]. Nevertheless, a primary obstacle to the successful blending of different plastics lies in their inherently lower interphase tension and lack of chemical compatibility, resulting in low-quality materials [8]. To address this issue, one potential strategy is to incorporate additives called compatibilizers during the melting process [9]. These compatibilizers facilitate interaction between the phases of two immiscible polymers, stabilize the morphology by reducing the drop size in the dispersed phase, and enhance the physico-mechanical properties of the mixture[3]. Traditional methods for achieving compatibilization involve adding small quantities of components, such as block or graft copolymers, fillers and coupling agents [2],[7]. This can be accomplished through either a chemical or physical process [1]. Reactive compatibilizers establish effective connections between polymers via reactive extrusion, while the physical dispersion of the copolymer segment in the phases of the mixture improves the interfacial adhesion [12].

Extensive analysis has been conducted on the compatibilization of different plastic wastes. Non-reactive block copolymers such as ethylene-propylene-diene copolymer (EPDM) and ethylene-propylene copolymer (EPM) have been employed to facilitate the compatibilization of recycled PP/PE [12]. Fortelny et al., demonstrated the effectiveness of combining these block copolymers with styrene-butadiene (SB) in PE/PP/ polystyrene (PS) blends, resulting in waste materials with comparable toughness to their virgin counterparts [16]. Another commonly investigated block copolymer is poly(styrene-b-(ethylene-co-butylene)-b-styrene) (SEBS), which has shown remarkable efficacy in improving the mechanical and morphological properties of immiscible blends such as high density polyethylene (HDPE)/PP [17], PP/high-impact polystyrene (HIPS) [18], and PET/HDPE [19]. Zhang et al., conducted research showing that the incorporation of SEBS results in a more stable and uniform morphology within the blend, while significantly enhancing the ductility of the blend when PET is combined with low-density polyethylene (LDPE) [20], [21]. Additionally, Inoya et al., demonstrated that the addition of 1 parts per hundred rubber SEBS improved the impact strength of unnotched specimens by 2.7 times and allowed for a reduction in drop size of approximately 50% in blends composed of 95% recycled polyethylene terephthalate (rPET) and 5% PP [22]. These findings highlight the advantageous effects of SEBS as a compatibilizer in this context.

Besides of physical compatibilization, reactive compatibilizers include functional groups that can chemically react with the polymers used in the blend. This allows the copolymer to interact with one of the phases while simultaneously reacting with the other. These interactions result in the formation of covalent bonds facilitated by reactive agents such as peroxide, anhydride, isocyanate and oxazoline [9]. In the waste stream, maleic anhydride (MA) and glycidyl methacrylate (GMA) are commonly employed due to their compatibility with hydroxyl, carboxyl, and amine functions [1], [12]. The use of various polyolefins and block copolymers grafted MA serving as a compatibilizer, results in notable improvements in the mechanical properties, morphology, and rheology of blends including recycled poly(acrylonitrile-co-butadiene-co-styrene) (ABS)/polycarbonate (PC) [23], recycled polyamide 6 (PA6)/ recycled polypropylene (rPP) [24], [25], rPP/nylon [26], and recycled high density polyethylene (rHDPE)/rPP [14], [27], [28]. Furthermore, MA has displayed effectiveness in the compatibilization of rPET with other PSW materials, showcasing the ability to react with hydroxyl ends on PET [29], [30], [31], [32], [33], [34], [35]. Similarly, GMA has been used in the compatibilization of rPET and rHDPE [36], [37], [38] and has demonstrated greater efficiency than MA, as it can react with both carboxyl and hydroxyl ends of PET [39], [40]. Additionally, GMA compatibilizers have also been used for the reactive compatibilization of others PET-Based blends, such as rPET /PA-11 blends [41], [42], [43] .

The most commonly used technique for the compatibilization of plastic waste involves utilizing an extruder to homogenize the plastic waste blend, followed by injection molding to create the desired products[1]. Single-screw and twin-screw compounders are typically employed for this purpose [44], [45], [46], [47], with twin-screw extrusion recognized as the most effective method. Over the past decade, material extrusion (MEX) additive manufacturing has experienced rapid growth owing to its simplicity, low cost, and capability to produce complex, customizable geometries. One such MEX technology is fused granular fabrication (FGF), which enables the direct printing of pellets or flakes derived from recycled waste materials. FGF utilizes a screw mechanism to convey the material to a heating element, where it is melted and then extruded through a nozzle. Additionally, with the rise of distributed recycling and additive manufacturing (DRAM), a new method enables waste plastic to be 3D printed into many objects [48], [49], [50]. Notably, PET has been demonstrated to be printable through DRAM method [51], this presents an innovative approach for achieving direct blending capabilities for multi-materials and facilitating the transformation into functional objects without the need for secondary processing, as required in conventional methods. The utilization of direct material extrusion 3D printing for this purpose, however, is still in its infancy. While there has been some exploration in blending recycled materials via large-scale direct 3D printing [52], [53], [54], the use of compatibilizers, particularly their direct addition during the printing process, remains largely unexplored. This is due to the lower mixing efficiency and shorter residence time compared to the twin-screw extrusion process.

The primary objectives of this study are to conduct a comparative analysis and evaluation of three SEBS-based compatibilizers, directly added during the FGF 3D printing process. Two of these compatibilizers facilitate only physical interactions, while one promotes reactive compatibilization. Additionally, the study aims to contribute to our understanding of the feasibility of large-scale 3D printing, specifically FGF, as a novel methodology for blending and compatibilizing PSW in one-step without prior sorting compared with the conventional two-step method using both twin-screw extrusion and injection molding. Furthermore, this research will contribute to the advancement of the DRAM approach and the development of more durable and compatible materials for 3D printing applications.

In the context of this research, a fully recycled water bottle was employed as a representative model. The bottle was composed of PET and HDPE for the body and cap, respectively, without prior separation. Obtained binary and ternary blends were then extensively analyzed for chemical, thermal, rheological, morphological, and mechanical properties.

2. Materials and Methods

2.1 Materials

In this study, post-consumers Cristaline water bottles composed of 90% PET for the body and 10% for the cap made of HDPE, were collected from receptacles placed in engineering schools in France. Kraton G-1650 and G-1652 kindly donated by Kraton Polymers (Almere, Netherlands) were used as non-reactive compatibilizers and will be named by their code G1650 and G1652, respectively. Both are linear SEBS copolymer including about 30 wt% of polystyrene units. Moreover, a maleated SEBS cirKular+ C1010 (C1010) donated by Univar Solutions (France) was used as a reactive compatiblizer. C1010 contains ~1.5% of grafted maleic anhydride. The primary properties of the three compatibilizers used in this study are shown in Table 1 [55]. It is worth to mention that molecular weight and the polydispersity index are not provided by the manufacturer as well as the Viscosity Brookfield of the C-1010 compatibilizer.

Table 1. Properties of the compatibilizers.

	G1650	G1652	C1010
Specific gravity	0.91	0.91	0.9
Viscosity Brookfield [cps] Sol (Toluene) 20.0\%w	8000	1800	-
Melt flow index [5kg-230°C][g/10min]	<1	5	34
Tensile [MPa]	35	31	-
Tensile [PSI]			390
Elongation at break [%]	500	500	361
Hardness shore A	70	70	62

2.2 Blending and sample preparation

Prior to the blending process, the material transformation into feedstock followed the methodology used in previous research [56]. Before each test, the rPET/rHDPE blends were dried in a conventional oven overnight at 60 °C to minimize moisture-induced degradation; however, it is noteworthy that compatibilizers were not subject to a drying process. Binary blends consisting of rPET/rHDPE (90:10 w/w), hereinafter referred to as rPET90/rHDPE10 and ternary blends involving rPET81/rHDPE9/G165010, rPET81/rHDPE9/G165210, and rPET81/rHDPE9/C101010,The 10 wt % of the compatibilizers was chosen based on the literature [57], were prepared using two distinct processes. First, the extrusion-injection (EI) process using a co-rotating twin-screw micro-compounder (DSM Xplore Instrument, Netherlands) and injection molding machine (DSM Xplore Instrument, Netherlands). Secondly, the printing process using a modified open-source FGF printer with three heat zones (Gigabot XL re:3D, Houston, TX, USA) [58]. For all the ternary blends the quantity of compatibilizer utilized was 10 wt%.

For the micro-compounder, the extrusion temperatures were set at 260 °C, while the screw speed was maintained at 100 rpm. These temperature conditions were selected to ensure material melting without causing degradation. The flow time through the extruder was carefully measured and was set at 1 minute, 2.2 minutes, and 5 minutes to explore the impact of residence time on the compatibilization process. Subsequently, the extrudates were injected into the mold using an injection machine operating at 260 °C, with the mold temperature held at 40 °C. Conversely, the ternary blends were directly produced through FGF printing. The residence time during extrusion within the machine was experimentally determined to be 2.2 minutes. Detailed printing parameters are given in Table 2.

Table 2. Samples FGF printer parameters.

Parameters	Value	Units
T1	264	°C
T2	230	°C
T3	220	°C
Tbed	84	°C
Width	2	mm
Speed	10	mm/s

Cooling	0	%
Infill density	100	%
Layer height	1	mm
Extrusion Multiplier	1.32	-
Nozzle diameter	1.75	mm
Walls/ Perimeters	1	
Raster angles	45	°
Build orientation	XZ	

2.3 Characterization Methods

The EI and printed samples of rPET90/rHDPE10 with 10 wt% of compatibilizer were characterized using different methods, as summarized in Table 3, which also provides the corresponding sample codes, and detailed in the following subsections.

Table 3. Summary of the sample preparation and characterization tests. SC: sample code, RT: residence time, NR: non-reactive, R: reactive, MC: microcompounder, GB: Gigabot, Min: minutes, MDSC: modulated differential scanning calorimetry, TGA: thermogravimetric analysis, SEM: scanning electron microscopy, FTIR: Fourier-transform infrared spectroscopy, MFI: melt-flow index.

SC	Compatibilizer		Machine		RT	Characterization							
	NR	R	MC	GB	Min	Mechanical		Thermal		Morphological	Chemical	Rheological	
						Tensile	Charpy	MDSC	TGA	SEM	FTIR	Dynamic	MFI
EI-W/O			x		1	x							
			x		2.2	x	x	x	x	x	x	x	
			x		5	x							
EI-G1650	G-1650		x		1	x							
	G-1650		x		2.2	x	x	x	x	x	x	x	
	G-1650		x		5	x							
EI-G1652	G-1652		x		1	x							
	G-1652		x		2.2	x	x	x	x	x	x	x	
	G-1652		x		5	x							
EI-C1010		C-1010	x		1	x							
		C-1010	x		2.2	x	x	x	x	x	x	x	
		C-1010	x		5	x							
P-W/O				x	2.2	x	x	x	x	x	x	x	x
P-G1650	G-1650			x	2.2	x	x	x	x	x	x	x	x
P-G1652	G-1652			x	2.2	x	x	x	x	x	x	x	x
P-C1010		C-1010		x	2.2	x	x	x	x	x	x	x	x

2.3.1 Residence time estimation

The length of time that the material passes through the extruder in the 3D printer was determined experimentally. For this, a small amount of pink tracer was introduced directly into the flakes within the rotating screw during a steady state extrusion process at a feed rate of 10 mm/s. The time elapsed until a noticeable color change occurred at the nozzle was carefully recorded. This procedure was performed at a printed speed of 10 mm/ s using 25 gr of material, and it was repeated four times to evaluate its reproducibility and consistency. For the GigabotX the residence time was determined to be approximately 2.2 min ± 0.12 and subsequently compared to the residence time measured in the micro-compounder, which varied between 1 to 5 minutes.

2.3.2 Fourier-transform infrared (FTIR) spectroscopy

A Bruker IFS 66 spectrophotometer was used for IR measurement. Each spectrum was recorded in the range of 4000 cm^{-1} to 375 cm^{-1}, with 32 scans per spectrum and a resolution of 4 cm^{-1}. Baseline correction, and normalization in the peak 1410 cm^{-1} [59] were carried out.

2.3.3 Modulated differential scanning calorimetry (MDSC)

Modulated differential scanning calorimetry analysis were performed with a DSC Q2000 (TA Instrument) at SAMPL - LRGP (Université de Lorraine-CNRS), operating under air atmosphere at heating rate of 10 °C/min and cooling rate 5 °C/min. For printed and EI samples, a small section was cut from the tensile bar. Neat polymers, binary and ternary blends were evaluated using three cycles: first heating from 20 °C to 300 °C, cooling to 20 °C and reheating to 300 °C for rPET. The rHDPE sample was analyzed following similar cycles but with a minimum temperature set at -70 °C and a maximum temperature set at 210 °C. Finally, binary and ternary blends were analyzed with temperatures ranging from -70 to 300 °C.

The first heating was made to erase the thermal history of the sample. The measurements of the thermal properties of the second melting curve.

The degree of crystallinity (Xc) was calculated from the area under the melting peaks as expressed in equation (1) [57], [60]:

$$Xc\ (\%) = \frac{\Delta H_m}{w\ x\ \Delta H_m^o} \times\ 100\% \qquad (1)$$

where, ΔH_m is the latent heat of fusion , w is weight percentage of polymer in the blend, and ΔH_m^o is the latent heat of fusion of 100 % crystalline PET (140J/g) and HDPE (293 J/g), respectively, which was provided in the literature [59], [60].

2.3.4 Rheology

The rheological analysis was carried out using two types of testing methods. First, the rotational rheometer was used to measure the complex viscosity, the storage modulus, and the loss modulus of EI and printed samples intended for tensile test with and without compatibilizers. Measurements were determined in a rheometer ARES (TA Instruments) using parallel plate geometry (d=25mm, gap=1.4mm) for frequencies ranging from 100 to 1 rad/s

with 5 points per decade measured from high to low under air atmosphere at 270 °C [61] for all samples and HDPE at 170 °C [62]. Afterwards, the melt flow index (MFI) of rPET90/rHDPE10 flakes dried two days before the test with and without compatibilizers was determined using an Instron CEAST MF20. The analysis was performed on two samples of ~5g at a temperature of 255°C with a 2.16 kg weight following the ASTM D1238 standard [63] and a previous study [56]. The average value of the results was reported in units of g/10min.

2.3.5 Scanning electron microscopy (SEM)

In order to gain a more comprehensive understanding of the morphological characteristics of the blend, samples underwent a Soxhlet extraction test to separate the minor phase HDPE within the blend. Samples intended for Charpy impact testing were fractured under cryogenic conditions using liquid nitrogen . The fractured pieces were then subjected to Soxhlet extraction in xylene at 80 °C for 14 h using a conventional Soxhlet apparatus. After extraction, the residual material was recovered, dried, and subsequently prepared for microstructural analysis. These samples were further prepared by sputter coating with a thin layer of platinum to facilitate improved observation. The samples were examined using a SEM (Hitachi model SU1000) with an operating acceleration voltage of 5 kV. Qualitative analysis of the images obtained was carried out. For each blend, at least 10 micrographs at ×600 magnification were processed using a Python-based image-analysis workflow to assess the homogenization of the mixture [60]. In each image, the algorithm automatically identified >300 droplets based on circularity and ellipticity criteria. The results obtained from each micrograph were then averaged, and mean ± standard deviation were calculated across the full image set per condition. These aggregated values were subsequently used to construct the normal distributions.

2.3.6 Mechanical characterization

2.3.6.1 Tensile test

Binary and ternary blends were tested for tensile properties according to the ISO 527-1 standard on type 1B [64] using a Zwick/Roell 1476 machine (L. Schreiner, Germany) with a load cell with capacity of 100kN. Measurements were carried out on five different specimens for each formulation at a loading speed of 10mm/min. After testing, the mean values and standard errors of stress, strain and Young's modulus were calculated and analyzed from the stress-strain curves obtained in the test.

2.3.6.2 Charpy test

Printed and EI samples were tested for impact properties in accordance with ISO 179-1-notched [65]on sample 1eAb in an 7.5J instrumented impact hammer (CEAST 9050, Instron). Measurements were made on ten different samples for each formulation selected.

3. Results and discussion

The primary objective of this study, was to assess the influence of compatibilization on the material properties of rPET and rHDPE blends produced via FGF printing process. Given the relatively short residence time (approximately 2 minutes) to achieve complete homogenization or allow significant interactions or reactions between the components in the printing process, various SEBS-based compatibilizers were tested. These included two non-reactive compatibilizer with different viscosities and molar masses to promote physical compatibilization, as well as one reactive compatibilizer grafted with MA for comparison.

Furthermore, due to the limited residence time during FGF, the printed samples (labeled as "P") were compared with samples prepared using micro-compounder followed by the extrusion injection molding (labeled "EI").

All analyses were performed on printed and EI samples with a residence time of 2.2 minutes. However, for the mechanical tests, the effect of the extended residence times in the micro-compounder, specifically 1 and 5 minutes was also evaluated.

3.1 Chemical analysis FTIR

From a chemical perspective, the potential interactions that presumably result from the addition of SEBS in the methylene group of the rHDPE and the aromatic ring of the rPET are shown in Fig. 1a. Additionally, the possible reaction of the hydroxyl groups of rPET with the anhydride group of SEBS-MA are presented in Fig. 1b. This possible compatibilization mechanism for physical and reactive compatibilizer on EI and printed samples was analyzed with FTIR and is shown in Fig. 2.

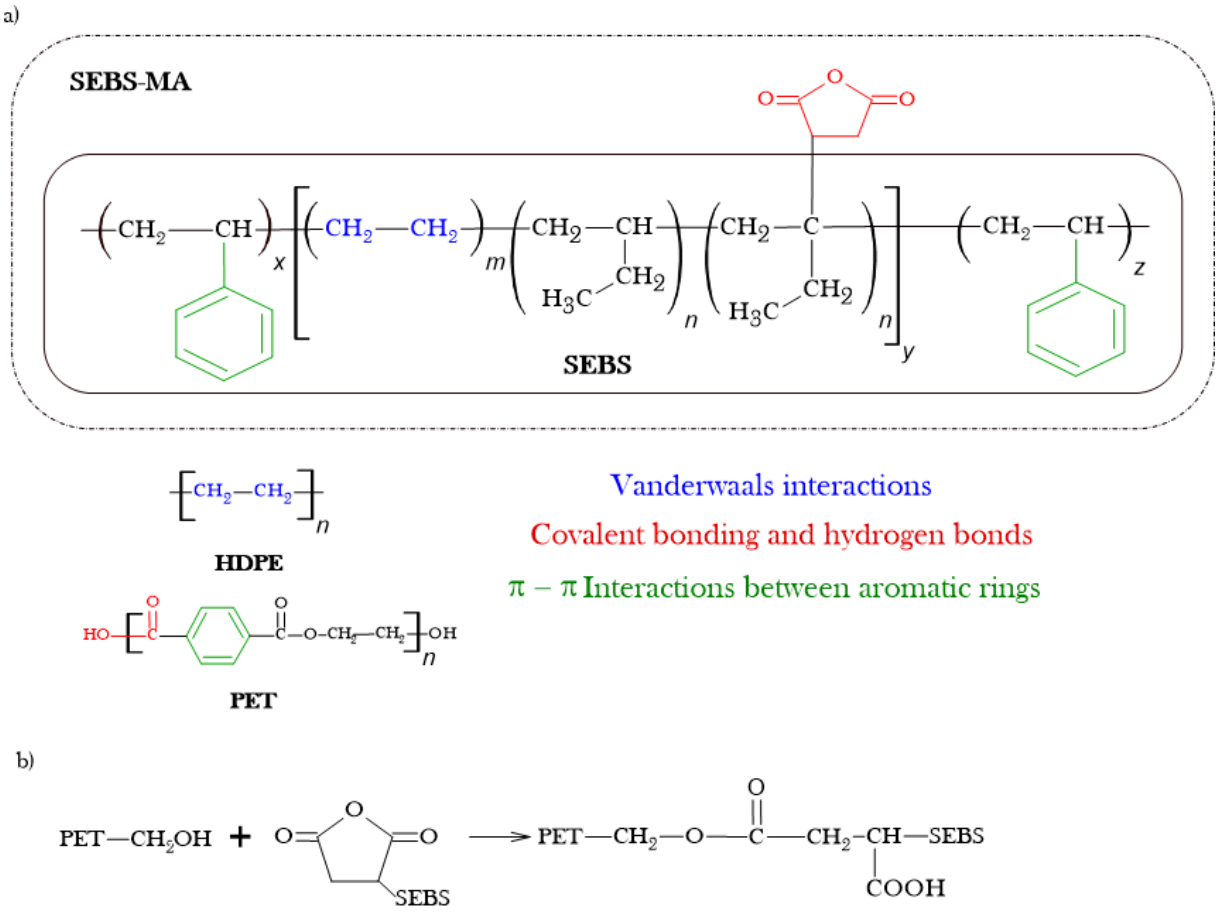

Figure 1. a) Chemical structure of SEBS, SEBS-MA, PET and HDPE with possible interaction (adapted from [66]). b) reaction of the terminal hydroxyl group of PET with maleic anhydride of the SEBS (adapted from [67]).

The characteristic peaks of PET attributed to C=O bond (1712 cm^{-1}), C-O ester (1240 cm^{-1}), CH_2 ester (1092 cm^{-1}), and CH_2 vibration (719 cm^{-1}) are notable in the binary and ternary blends

of both printed and EI samples (Fig. 2). In Figure 2, an increase of the intensity and appearance of peaks in 2960 cm^{-1}, 2918 cm^{-1}, 2849 cm^{-1}, and 698 cm^{-1} bands is also observed, which corresponds to the stretching of $CH/CH_2/CH_3$ groups. These bands are characteristic of both HDPE and SEBS, suggesting higher concentrations in those functional groups in the blend. Other than that, the main bands of rPET overlapped with those of the other components in the blends, making it challenging to observe the changes in the spectra. This overlap is primarily due to the high proportion of PET in the blend, which constitutes 90% of the material.

However, between 1480 cm^{-1} and 1440 cm^{-1}, two emerging peaks (1472 cm^{-1} and 1456 cm^{-1}) are observed with the addition of HDPE and compatibilizers, as shown in Fig. 2b. According to the literature, bands at 1470 cm^{-1} and 1450 cm^{-1} correspond to the trans (crystalline) and cis (amorphous) phases of the ethylene glycol group in PET [59], [68]. For the EI samples, the intensity of the 1472 cm^{-1} peak is lower compared to the printed samples, suggesting a suboptimal crystal structural formation due to the injection process. Additionally, Cobbs and Burton [69], utilized the bands at 1340 cm^{-1} and 972 cm^{-1} to observe such crystallization, as both are associated with the trans phase of PET. In Fig. 2b-c, it can be seen that the intensity of these peaks is greater for the printed elements compared to the EI ones. This change of FTIR bands around 1472/1456 cm^{-1} and trans-phase bands (1340/972 cm^{-1}) is indeed not due to a an overlap with HDPE/SEBS. This confirms the hypothesis that the increase in crystalline phase is a result of the 3D printing process, as later confirmed by DSC results. This process based on layer-by-layer deposition technique, that enables slower cooling rates, allowing polymer chains to have optimal crystalline arrangement compared to the rapid cooling rates characteristic of the injection molding process. Regarding the reactive compatibilization, the FTIR spectra of C-1010 display a peak at 1712 cm^{-1}, associated with the carboxyl group of the MA. However, the identification of the reaction between the carboxyl group of MA and the terminal hydroxy groups of rPET during extrusion was proved to be challenging [70]. This difficulty arises from the position of the peak and the low concentration of MA in both the compatibilizer and the blend, as observed in the results, where the characteristic band of MA was absent.

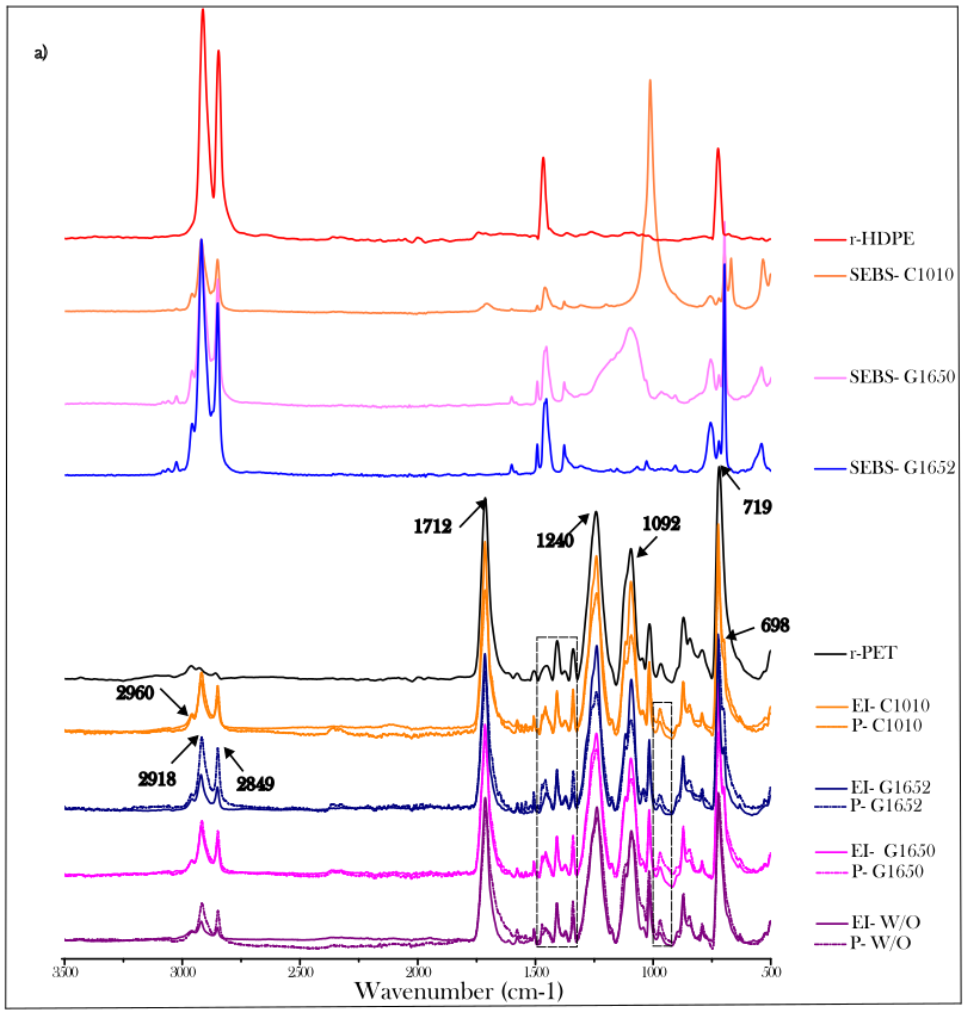
a)
r-HDPE
SEBS- C1010
SEBS- G1650
SEBS- G1652
1712
1240
1092
719
698
r-PET
2960
EI- C1010
P- C1010
2918
2849
EI- G1652
P- G1652
EI- G1650
P- G1650
EI- W/O
P- W/O
3500
3000
2500
2000
1500
1000
500
Wavenumber (cm-1)

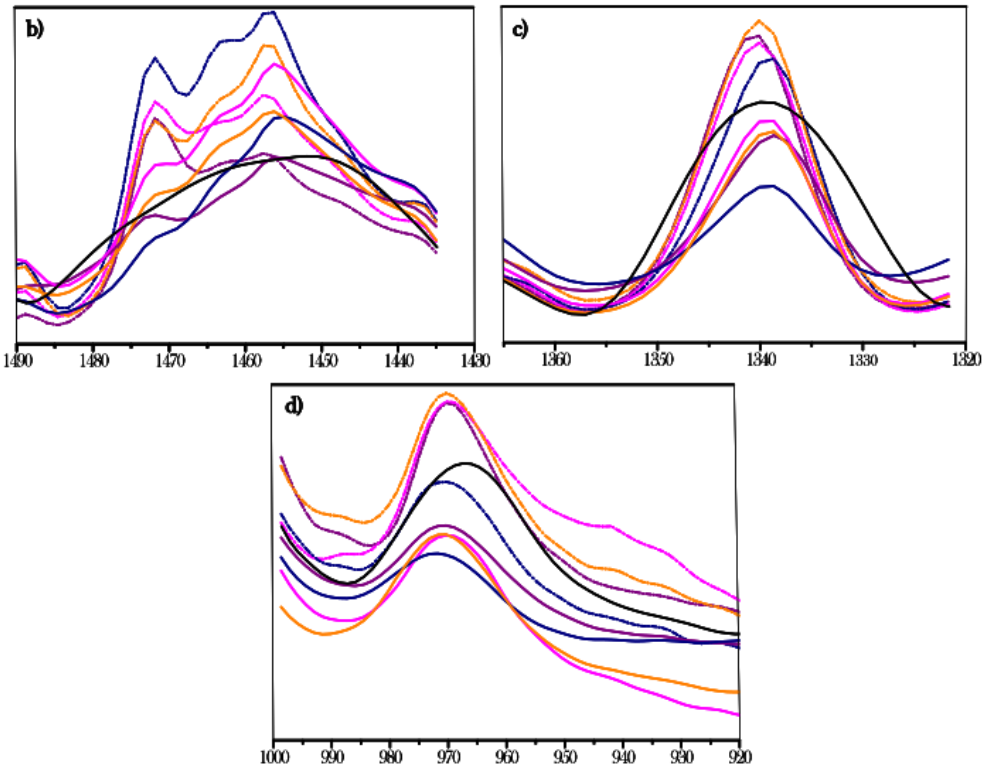

Figure 2. FTIR spectra revealing compatibilization mechanisms. a) FTIR spectra of individual components, binary, and ternary blends; Printed and EI samples with and without compatibilizers in region b) from 1490 cm^{-1} to 1430 cm^{-1}, c) from 1360 cm^{-1} to 1320 cm^{-1}, d) from 1000 cm^{-1} to 920 cm^{-1}.

3.2 Thermal analysis – DSC –

The thermal analysis of the binary and ternary blends, reveals two distinct peaks in the thermograms for both the first and second heating cycle depicted in Fig. 3. These peaks correspond to the melting temperatures of rPET and rHDPE, indicating the immiscibility between the two polymers [57]. The addition of rHDPE and compatibilizers did not have a significantly impact in the degree of crystallization nor in the glass transition of rPET, Table 4. However, in the second heating cycle, two rPET melting peaks appear in both printed and EI specimens. These variations in the melting peaks are associated with the partial melting and reorganization of the material's crystals or the existence of different crystalline phases [10], [71], [72] [73].

In the case of printed materials, the less intense rPET melting peak at lower temperatures suggests variations in the distribution of crystallite sizes, as previously observed in extruder PET [74], leading to the formation of imperfect crystals [75]. Conversely, an intense rPET fusion peak at higher temperature, could be attributed to perfect crystal formation, and may reflect a more efficient and less degraded material [75], [76]. In contrast, in EI samples, the same two peaks are observed, with a predominance of the peak corresponding to imperfect crystals at lower temperatures. The formation of these imperfect crystals may be attributed to the more traumatic nature of the injection molding process on the polymer chains compared to the 3D printing process. The results explain that printed materials exhibit higher average fusion

temperatures, reflecting better crystal formation. In contrast, injected materials tend to form more imperfect crystals at lower fusion temperatures. This arises from the increased degradation experienced during injection process, resulting in higher chain mobility due to the presence of shorter chain molecules formed by chain scissions. These findings are supported by thermograms obtained from the TGA. The analysis shows that degradation occurs earlier in the EI samples compared to the printed samples linked to degradation mechanisms initiated by the ends of chains (Fig. S1, supporting information).

Additionally, during the first heating cycle, the observation of cold crystallization in EI samples supports the hypothesis that the rapid cooling kinetics of the injection process result in partial crystallization, leading to the formation of less organized (imperfect) crystalline structures. Contrary, the absence of cold crystallization in the printed samples indicates that complete crystallization occurs during material deposition, resulting in more organized (perfect) crystalline structures. This phenomenon may also explain the observed increase in crystallization-related peaks in the FTIR spectra and in the Xc %, which was found to be slightly higher for the printed samples compared to the EI specimens (Table S2, Supporting Information).

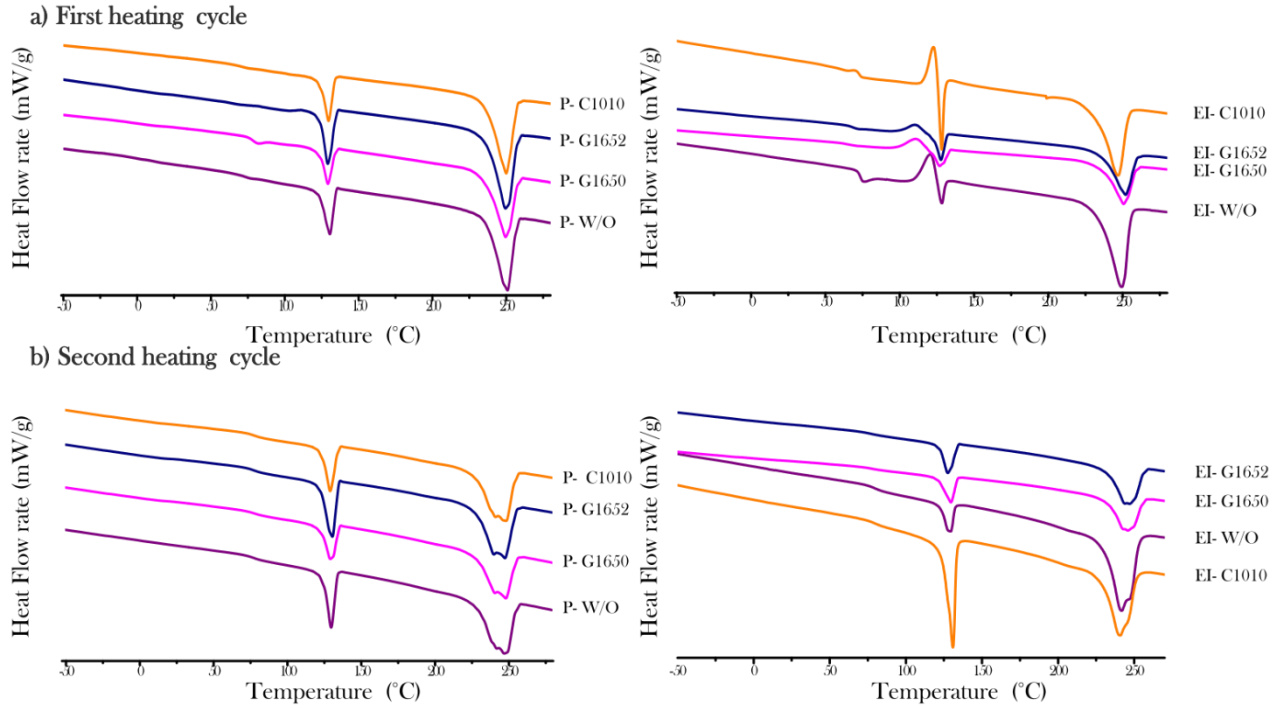

Figure 3. First and second heating endothermic thermograms of binary and ternary blends.

Table 4. Thermal analysis of rPET, rHDPE, binary, and ternary blends.

		Tm (°C)	Tc (°C)	Xc (%)

	Tg (°C)	rHDPE	rPET		rHDPE	rPET	rPET
rPET	78.7			244.8		208.5	33.0
rHDPE		131.0			120.0		
EI-W/O	79.3	130.0	241.7	243.5	116.6	201.8	24.0
EI-G1650	78.1	129.6		245.9	117.4	204.6	24.8
EI-G1652	75.9	127.5		243.9	116.5	209.6	22.8
EI-C1010	80.3	130.9	240.5	249.6	119.7	200.6	23.1
P-W/O	78.4	130.3	242.7	247.5	119.7	200.0	24.5
P-G1650	77.7	129.0	241.1	248.9	119.0	199.6	22.4
P-G1652	77.0	131.0	240.4	247.9	119.3	197.2	21.8
P-C1010	78.0	129.5	241.6	248.7	119.7	198.2	22.0

3.3 Rheology

Understanding the viscoelastic properties of materials is crucial for the 3D printing process, as these properties provide valuable insights into printability, deposition control, and interlayer adhesion [77]. To evaluate the rheological behavior of the blends, two methodologies have been used. An assessment of the flowability at low shear rate of the material rPET90/rHDPE10 with the addition of 10% of each compatibilizer was conducted via MFI measurement (Fig.4). The results indicate that the addition of the studied compatibilizers can either decrease or increase the MFI depending on the type of compatibilizer. The addition of G-1650 and G-1652 resulted in a decrease in material's MFI by approximately 47% and 10%, respectively. The substantial increase in viscosity observed with G-1650 can likely be attributed to the high intrinsic viscosity of the compatibilizer alone, which suggests a high molecular weight and longer polymer chains [78]. Conversely, the addition of C-1010 led to a slight increase in MFI by 6%, possibly due to the compatibilizer's high MFI of 34 g/10 min (low viscosity). These findings imply that the printing parameters, particularly the temperature, should be optimized for each material depending on the specific compatibilizer used. Although the samples in this study were printed at the same temperature to ensure comparability, the results and subsequent printing trials showed the need to adjust the printer settings according to the compatibilizer used.

To continue the rheological study, the flow and the behavior at high shear rate of the material were investigated using a conventional rheometer equipped with a parallel plate geometry. The tensile test specimens have been analyzed with the purpose of evaluate the impact of compatibilizers on the rPET90/rHDPE10 blend. As illustrated in Fig. 4, the complex viscosity of all components slightly decrease with increasing frequency, indicating non-Newtonian behavior and typical shear-thinning behavior of viscoelastic material [79]. The addition of compatibilizers leads to an increase in the viscosity of the ternary blends compared to the binary blend, which exhibits a viscosity value comparable to those of rPET. This suggests a limited interaction between the polymers in the binary blend, whereas the addition of a compatibilizer enhances the interaction between the polymer components, thereby improving the overall viscosity of the system. The increase in complex viscosity is especially pronounced in the EI-G1652 sample and both the printed and EI-G1650 samples across both high and low frequency ranges. This effect is likely attributed to internal molecular interactions between the polymers and, the compatibilizer viscosity, or potential degradation caused by rHDPE crosslinking [80].

The potential reaction between the C-1010 compatibilizer and the rPET may have slightly increased the viscosity at high frequencies. However, the high flowability of C-1010 likely

compensates this effect, as observed in the MFI measurements. This minor increase, may suggest that chain scission of rHDPE occurred as the material experienced degradation during processing [81],[82],[80]. This hypothesis is further supported by the TGA analysis, where early degradation occurs in samples compatibilized with C-1010 (Fig.S1, Supporting information). A sudden increase in viscosity at lower frequencies was observed and may indicate a reaction between the carboxyl end group of rPET and MA, which could occur more readily at lower shear rates due to the extended time available for interaction [82].

Viscosity did not show a significant change between printed and EI samples, with the exception of the G-1652 sample, where the EI specimen exhibited a noticeable difference. This observation could be influenced by the crosslinking of rHDPE, leading to increased viscosity [81], possibly due to the processing conditions or the fact that the tests were conducted under conditions similar to the printing process. It is therefore recommended that further studies be conducted under nitrogen conditions, in order to achieve a more complete understanding of this behavior.

Additionally, the inclusion of compatibilizers shifted both storage modulus (G') and the loss modulus (G") to higher values, indicating an enhancement in the material's elastic properties (Fig.S2, Supporting information). This effect is likely linked to the presence of the elastomeric phase, as observed in similar studies where the addition of rubber impact modifiers resulted in increased stiffness and elasticity [83].

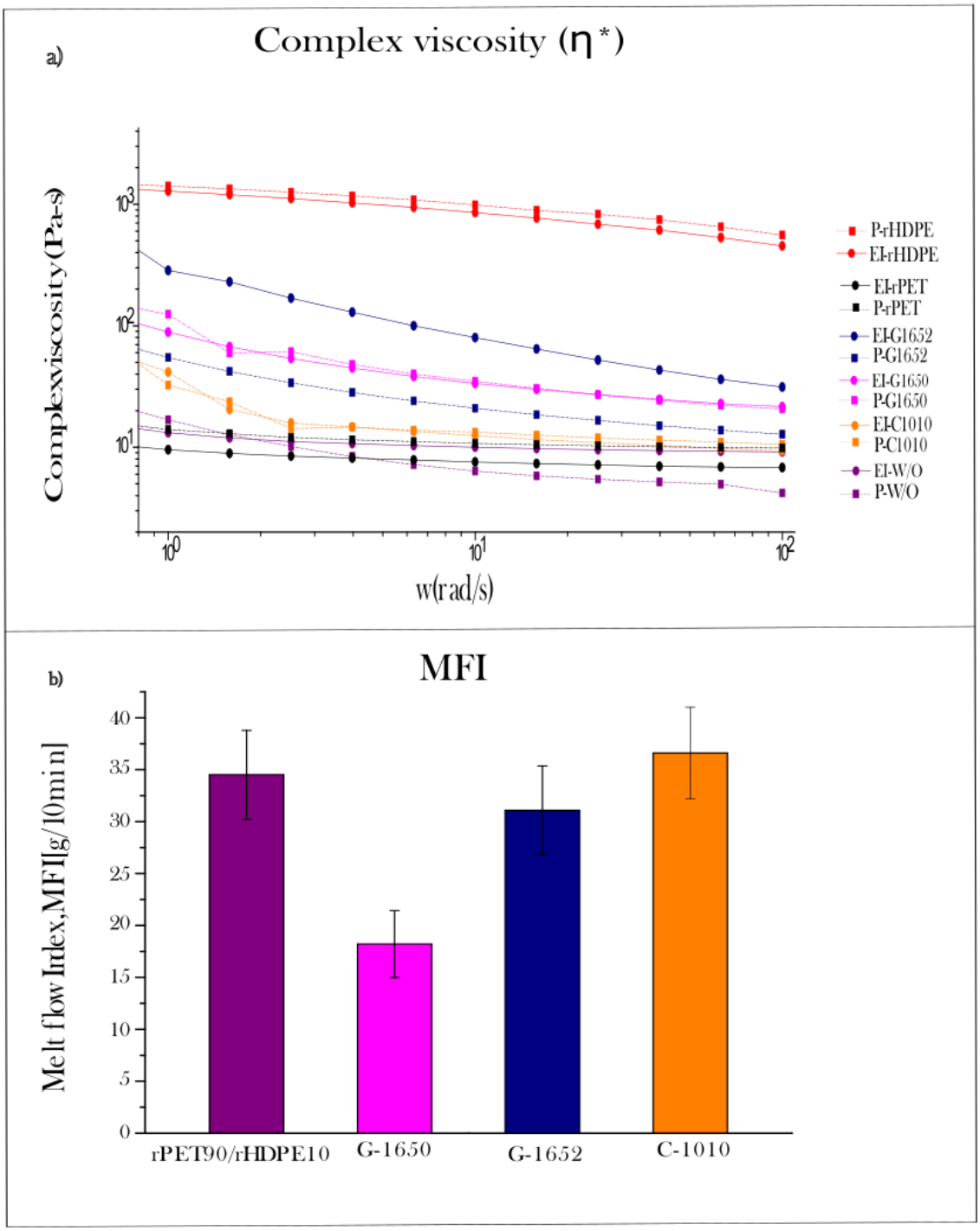

Figure 4. Rheological analysis of binary and ternary blends, a) complex viscosity, b)Melt flow index.

3.4 Morphology analysis –SEM –

SEM micrographs of both non-compatibilized and compatibilized blends of EI, as well as printed samples before and after Soxhlet extraction, are presented in Figures 5 and 6, respectively. In all images it can be seen that the HDPE and SEBS was dispersed in the phase of rPET matrix forming two-phase morphology due to low adhesion at the interface of both

materials [46]. EI and printed samples systems with compatibilizers, generally exhibited smaller phase dispersion and particle sizes, indicating enhanced phase interaction. This trend was consistent across all samples, with the exception of the non-compatibilized EI blend, which exhibited slightly smaller droplets compared to those observed in the C-1010 system.

In case of EI samples, the non-reactive compatibilizers displayed a more irregular morphology, particularly in the case of G1650, making direct comparisons more difficult (Fig 5.a). As illustrated in Figures 5c and 5d, the dispersed HDPE particles were encapsulated by the corresponding compatibilizers, forming core/shell structures, consistent with findings from similar studies [18], [78]. With the addition of G-1652, the HDPE is dissolved in SEBS and rPET droplets enter to the dispersed phase forming a salami structure (Fig 5.c). This may explain the augmentation in the viscosity of the material as seen in the rheological studies. Similarly, the addition of C-1010 formed more finer and dispersed salami structures (Fig 5.d). In the case of G-1650, fewer voids are observed, however, the surface exhibits greater heterogeneity and roughness, with broader particle dispersion and larger particle size. Additionally, phase separation is still visible, showing that SEBS G-1650 does not completely eliminate immiscibility (Fig. 5.a).

The examination of printed specimens reveals the formation of larger and more irregular void, showing a phase that appeared less dispersed, with HDPE and SEBS droplets deforming into a more fibrous structure (Fig. 6.a). This deformation is likely due to the limited time for HDPE to dissolve in SEBS, resulting in separate phases of the components. This can be attributed to the use of a single-screw extruder in the printing process, which provides only one surface or mixing point. In contrast, a twin-screw extruder offers four mixing points, leading to enhanced homogenization of the blend [84]. A single mixing point often results in non-uniform shear distribution, which can hinder the effective breakdown of polymer domains and the uniform distribution of compatibilizers. This inefficiency is primarily due to the localized concentration of shear, which fails to adequately disperse the components throughout the mixture [85], [86].

In order to facilitate more accurate qualitative analysis, Soxhlet extraction was performed to extract the minor HDPE phase, allowing for more precise measurements. The average droplet diameter was used for qualitative comparisons of the morphologies. This analysis confirmed the droplet dispersion (Figs. 5b, 6b). Additionally, demonstrated that the level of adhesion between both materials varies depending on the compatibilizer and the processing method used, as evidenced by the differences in particle size distribution (Fig. 7).

After Soxhlet extraction, it was observed that the addition of compatibilizer C-1010 led to a substantial reduction in average droplet diameter compared to the addition of G-1650 and G-1652 in the EI samples (Fig. 5.b). This reduction in droplet size suggests improved compatibilization and better integration of the compatibilizer, likely due to a decrease in interfacial tension. Additionally, this could be another indication of chemical reaction between the MA functional group and the hydroxyl end groups of PET, as well as the probable affinity between SEBS and polyolefins [87]. These findings are reflected not only in the reduced droplet size but also in the enhanced elastic properties of the material, as it will be discussed subsequently. Additionally, in cases where the rPET does not react with the compatibilizer, it is likely that Soxhlet extraction removes both the HDPE and SEBS phases. This observation may explain the larger particle sizes in specimens with compatibilizers compared to those without, as noted in the EI samples (Fig 7).

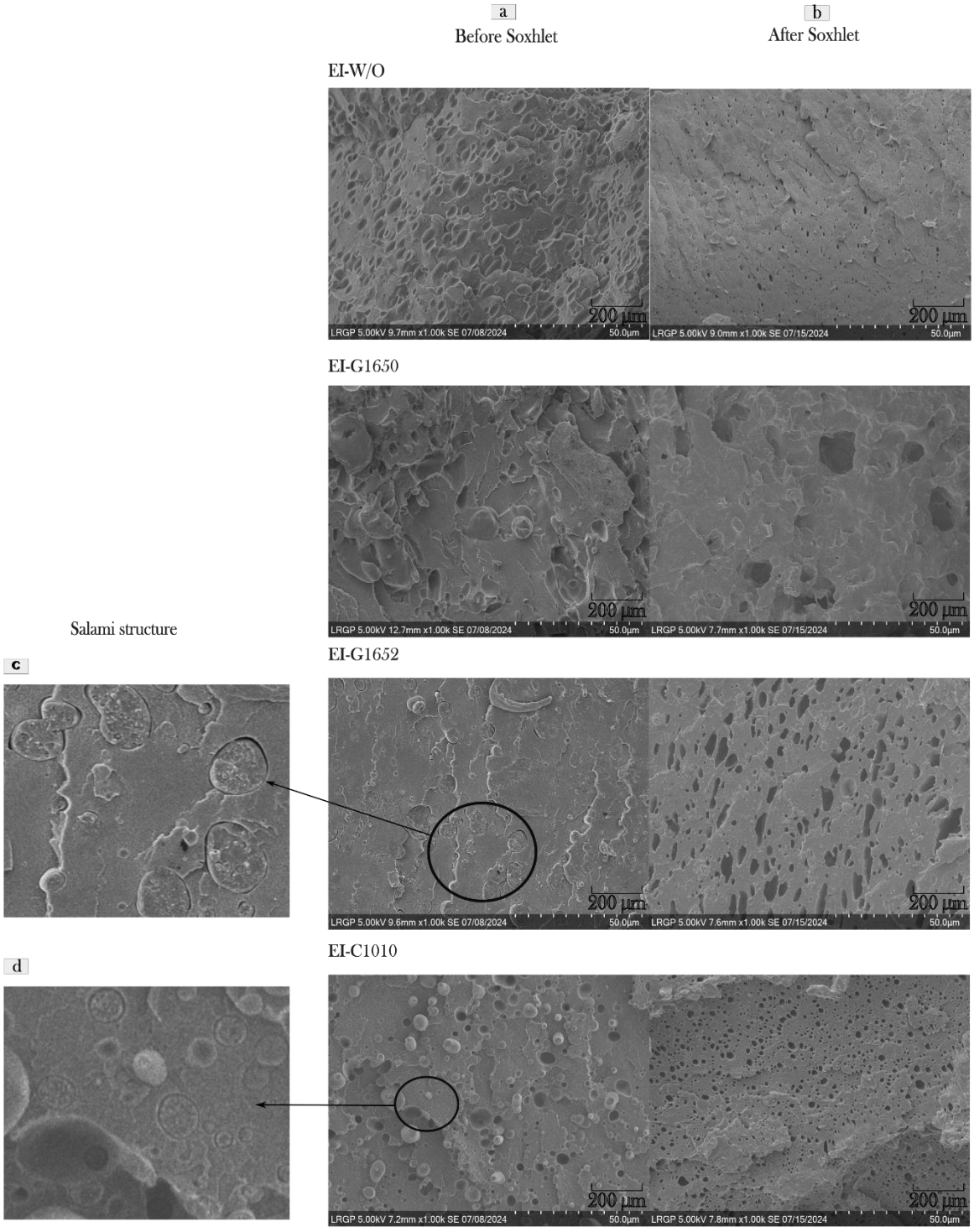

Figure 5. SEM micrographs x1K of EI samples: a) before, b) after Soxhlet extraction , and salami structures with addition of c) G-1652, d) C-1010

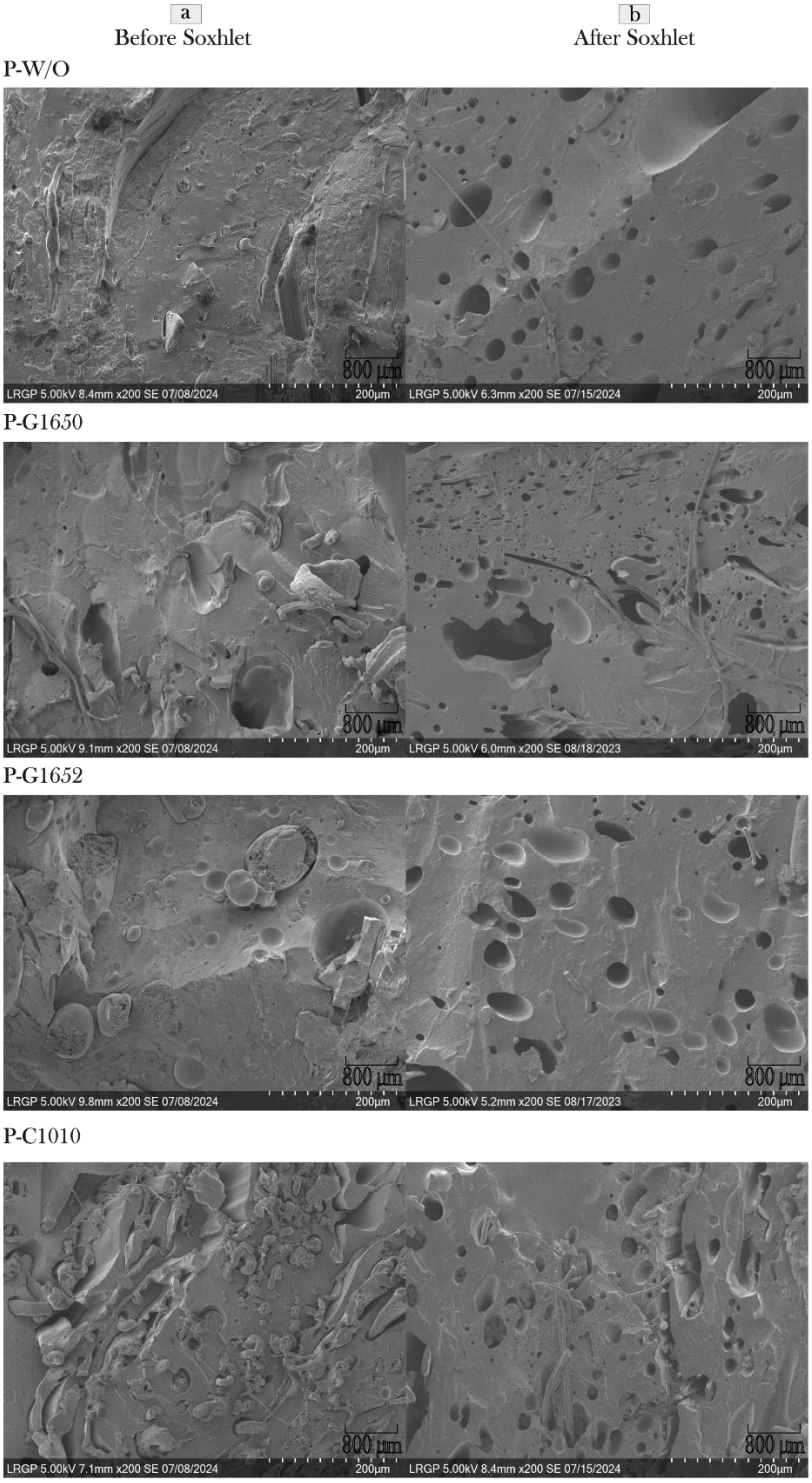

Figure 6. SEM micrographs x200 of printed samples: a) before, b) after Soxhlet.

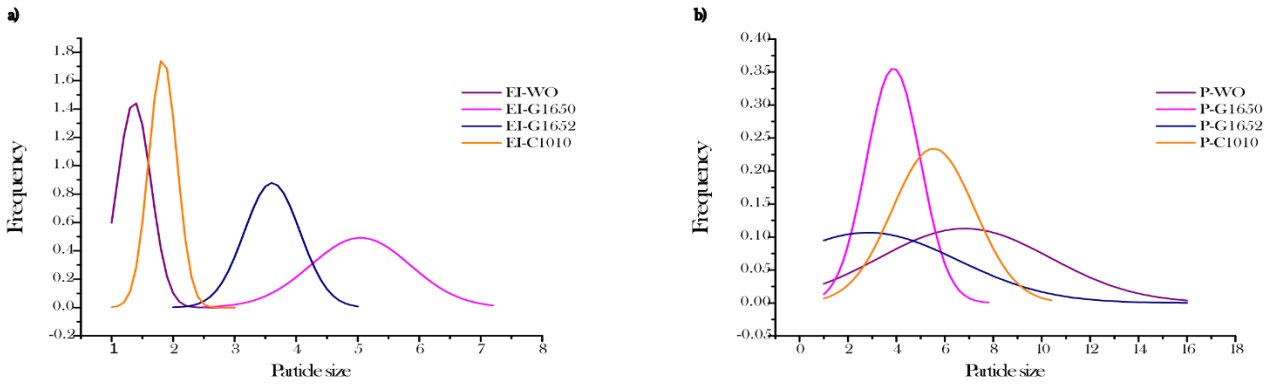

Figure 7. Particles size distribution a) EI samples, b) Printed samples, with and without compatibilizers.

3.5 Mechanical analysis

Within the compatibilization process, particularly in reactive extrusion, the duration of the reaction is intricately linked to the duration necessary for the material to traverse the extruder [88]. Thus, in the first part of this section, the potential impact of residence time on the manufactured EI specimens in the absence or presence of a compatibilizer was assessed. For this assessment, the materials were blended in a twin-screw micro-compounder with three specific residence times: 1 minute, 5 minutes, and 2.2 minutes. Results are depicted in the box plot in figure 8 and mean values of mechanical tensile test are presented in (Table. S2, Supporting information).

Results indicate that without a compatibilizer, specimens exhibited higher strength and elastic modulus, regardless of the duration of residence time. This outcome was anticipated since the addition of impact modifiers or rubber-type compatibilizers as SEBS typically results in a decrease in mechanical properties [83], [89],[90], [91]. Specimens with a one-minute residence time generally demonstrated slightly superior strength and Young's modulus compared to those subjected to longer residence times. This effect was particularly noticeable in specimens containing G-1650, where prolonged processing times may have led to accelerated thermal degradation, potentially due to the crosslinking of the rHDPE [81], [82]. Another possible explanation is that the higher viscosity of G-1650 may hinder proper mixing and adhesion with the matrix, leading to the formation of large and heterogeneous domains, as observed in the SEM analysis.

In contrast, specimens containing the C-1010 compatibilizer, maintained a median strength of 37.4 ± 1.5 MPa, regardless of residence of time. Additionally, specimens with C-1010 and G-1652 performed elongation without rupture, indicating improved ductility. This improvement is likely attributed to the lower viscosity of these compatibilizers compared to G-1650 [92], as well as potential mechanisms such as crack deflection, debonding, or microcracking, which contribute to increased toughness through energy absorption [93], [94], [95]. However, the observed reduction in tensile strength may be attributed to these same mechanisms or to the formation of cavities, as observed in the morphological analysis. The presence of smaller particles size and cavity formation could act as stress concentration points, thereby facilitating fracture propagation [96].

Regarding the elastic modulus, the incorporation of SEBS into the specimens resulted in an average reduction of approximately 23 ± 6.4% compared to non-compatibilized specimens.

This decrease in modulus suggests a softer and ductile material property, consistent with the rubber-like nature of SEBS [97]. Both the tensile test and Young's modulus follow a similar pattern. However, it is evident that the mechanical properties vary depending on the type of compatibilizer used.

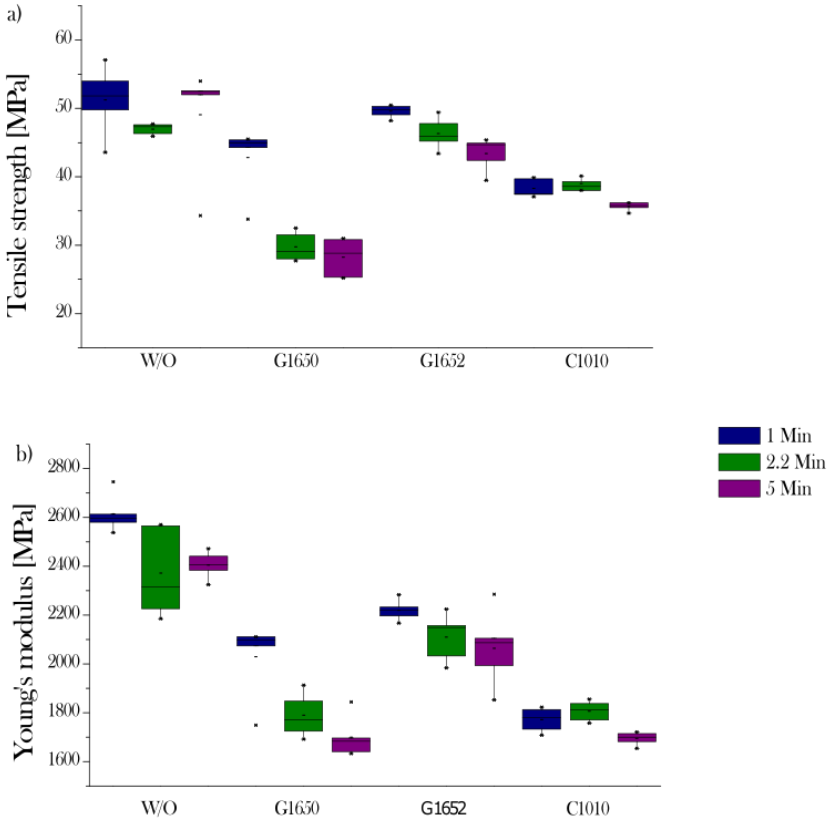

Figure 8. Mechanical properties of injected samples changing the residence time a) Tensile strength b) Young's modulus.

To conduct a comparative analysis between the conventional blending method and the novel direct printing technique, the injected samples with a residence time of 2.2 minutes were compared with the printed samples that were subjected to the same residence time, as determined using experimental means. Mean values are presented in Table 6.

Table 6. Mean values ± SD of mechanical properties of injected and printed samples at 2 min.

Sample	Tensile strength	Young's Modulus	Tensile strain	Nominal strain	Impact strength
	σ [MPa]	E [GPa]	[mm/mm]	[mm/mm]	[KJ/m^2]
EI-W/O	47 ± 0.8	2.4 ± 0.184	0.0295 ± 0.0018	0.0303 ± 0.0020	0.9 ±0.3
EI-G1650	29.8 ± 2.1	1.8 ± 0.0904	0.0206 ± 0.0034	0.0210 ± 0.0036	1 ± 0.5
EI-G1652	46.2 ± 2.3	2.1 ± 0.098	0.0350 ± 0.0015	0.5983 ± 0.3383	1.1 ± 0.4
EI-C1010	39± 2.9	1.8 ± 0.042	0.0331 ± 0.00036	0.8892 ± 0.4245	0.9 ± 0.1
P-W/O	23.3 ± 6.1	2.1 ± 0.091	0.0102 ± 0.0013	0.0114 ± 0.0011	0.67 ± 0.1

P-G1650	12.9 ± 5.6	1.5 ± 0.171	0.0081 ± 0.0020	0.0085 ± 0.0028	0.84 ± 0.2
P-G1652	25.3 ± 2.6	1.8 ± 0.244	0.0157 ± 0.0019	0.0167 ± 0.0023	0.92 ± 0.3
P-C1010	24.6 ± 1.7	1.6 ± 0.174	0.018 ± 0.0028	0.0188 ± 0.0030	1.5 ± 0.6

The results depicted in Fig. 9a-b reveal a significant increase in tensile strength and Young's modulus in EI samples, showing enhancements ranging between 35% to 50% and 5% to 14%, respectively, when compared to 3D printed samples. This outcome is consistent with literature findings, which attribute such differences to the inherent characteristics of 3D prints. Specifically, the presence of air gaps in the diamond-shaped areas, influenced by various factors such as process parameters, materials, and coloring additives between layers, contributes to weakness in the printed samples [98].

This discrepancy is particularly pronounced in non-compatibilized blends and those treated with G-1650, compared to G-1652 and C-1010. The utilization of G-1652 favored the mechanical properties of the blends, resulting in higher strength to that achieved with C-1010, while G-1650 exhibited brittleness and lower stiffness.

The favorable effect in the addition of compatibilizers is evident when analyzing the stress vs. strain curve (Fig. 9d). It is evident that most samples experienced immediate rupture, except for those treated with G-1652 and C-1010 compatibilizers. The increase in the elongation at break was reported before. Iniguez et al., reported that the addition of 10% of G-1652 significantly increased the elongation at break of post-consumer PET and HDPE blends [19]. This may be due to their lower molecular weight, which allows the mobility of the polymer chain promoting better interaction and the contribution to the toughening effect provided by both compatibilizers, as previously discussed. Interestingly, in the printed samples, a rupture occurred immediately regardless of the added compatibilizer where the nominal strain at break closely mirrored the tensile strain (Table 6). This indicates a need to improve the processes, parameters, or the machine itself. Implementing a screw mechanism that allows for better blending, such as a double-screw extrusion system, could be beneficial. Additionally, literature has reported that planetary roller extruders achieve superior blending, making them an interesting option to incorporate into 3D printers [84]. Additionally, the use of a large diameter nozzle may introduce more voids within the sample, thereby reducing its mechanical properties and increasing its brittleness.

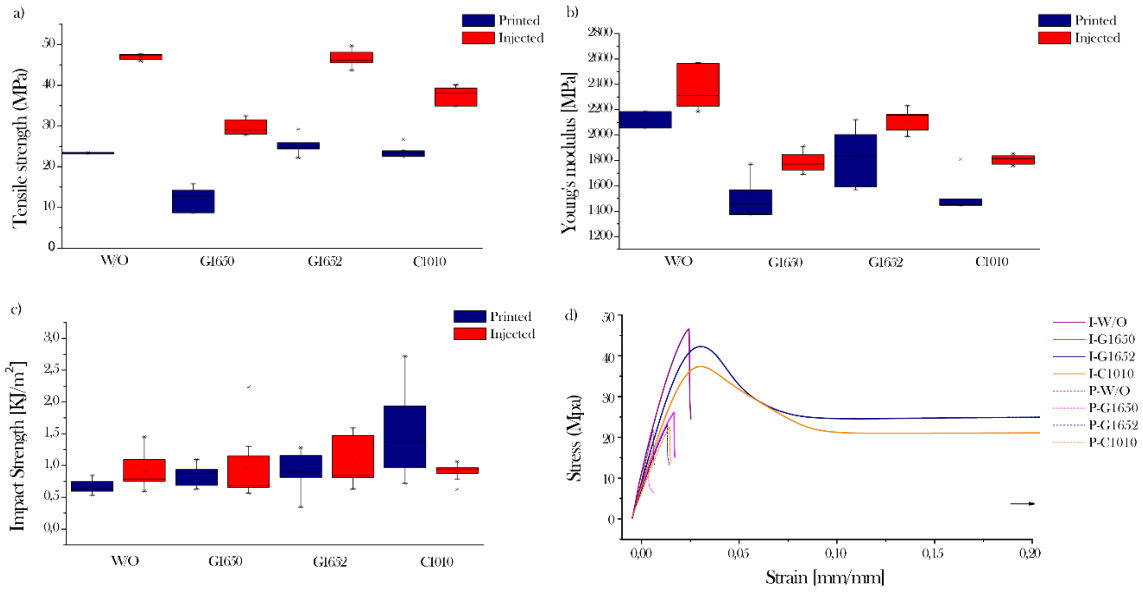

Figure 9. a) Tensile Strength; b) Young's Modulus; c) Impact strength; d) Tensile test curves of the injected and printed samples with 2.2 min residence time.

The impact strength results, as shown in Fig. 9c, reveal a slight variation between printed and injected samples. EI specimens demonstrated approximately a 20% higher impact strength compared to their printed counterparts, with the exception of the C-1010 samples. This suggests that the injection molding process generally enhances impact resistance, possibly due to better material consolidation and fewer voids. The results show that both printed and injected samples benefit from the inclusion of compatibilizers, which enhance the material's ability to absorb impact energy. Printed C-1010 showed the higher impact strength of 1.5 ± 0.6 KJ/ m², however the most variable results. In the case of injected samples, G-1652 exhibits the highest impact strength of 1.1 ± 0.4 kJ/m². Similar impact results for PET/HDPE blends where found in the literature [99].

The results of the mechanical tests, it is evident that compatibilizers G-1652 and C-1010 performed elongation at break, leading to an augmentation of the ductility. The variation observed among compatibilizers can be attributed to the higher mobility of G-1652 polymer chains, owing to a lower molar mass, facilitated a more effective dispersion of HDPE in PET. This improved the mechanical properties by enhancing the interfacial interaction between the materials. Additionally, MA in C-1010 may enabled the reaction between the hydroxyl ends of the PET molecules. However, further testing is required to confirm this hypothesis.

In essence, the distinct mechanisms of action-enhanced dispersion and chemical interaction underlie the effectiveness of G-1652 and C-1010, respectively, in improving the mechanical properties of the blend of injected samples. This improvement can be attributed to the use of twin-screw extrusion and injection molding, which produce fully dense parts, in contrast to 3D-printed samples that contain voids due to the layer-by-layer deposition process. Additionally, the reduced properties observed in the 3D printed samples can be attributed to several factors, including the limitations inherent in the single-screw system, inadequate mixing time, suboptimal printing parameters, and inherent constraints of the 3D printing process.

4. Conclusion and future work

This study highlights the role of compatibilizers in enhancing the properties of rPET and rHDPE blends using two distinct processing methods: conventional extrusion-injection molding and large-scale FGF 3D printing. The results showed that the compatibilizers improves phase interaction, increasing the elongation at break by ~40 %, enhancing rheological behavior by reducing the MFI between 10 % and 47 %, depending on the compatibilizer used, and improving the morphological properties in EI samples. In contrast, printed samples exhibited less degradation and a more crystalline structure at elevated temperatures, as confirmed by FTIR and DSC-TGA analyses. However, the mechanical properties of the printed samples were ~50 % inferior than those of the EI, primarily due to suboptimal layer adhesion, void formation, and insufficient material homogenization.

Morphological analysis revealed greater particle size reduction in blends processed through EI. Nonetheless, two-phase separation and a core-shell structure were still observed. The compatibilizer C-1010 showed notable efficacy, particularly in enhancing the ductility of the blends. Additionally, C-1010 exhibited greater particle size reduction. In contrast, G-1650 demonstrated weaker mechanical performance, likely due to its higher molecular weight and limited ability to form finely dispersed structures.

While injection molding remains a well-established technology, the direct 3D printing process still faces challenges in achieving consistent material properties. The single-screw extrusion mechanism of the FGF printer limits blend homogenization and reduces compatibilizer effectiveness. Nevertheless, this approach holds promise for recycling multi-material blends and can be optimized through more reliable printing methods, including the implementation of a twin-screw or planetary roller extruder to enhance blend homogenization [84]. Additionally, refining printing parameters adapted to the compatibilizers could further enhance the mechanical properties and consistency of printed objects. Future work should also investigate the recyclability of printed materials over multiple cycles, assess the environmental and economical feasibility of using FGF to process post-consumer plastic waste. Expanding this approach to other common plastics such as PP, LDPE, PS could expand its applicability of this method. This would require re-optimizing the compatibilizer system and adjusting printing parameters to account for the different processing behaviors of these polymers.

Declaration of competing

The authors declare that they have no known competing financial interest or personal relationships that could have appeared to influence the work reported in this paper.

Acknowledgements

The authors would thank the LUE program for the financing of the thesis, the Lorraine Fab Living lab platform, and the Thompson Endowment. Additionally, authors want to thank Philippe Marchal for the scientific support, Richard Laine for the technical support, Maud Lebrun, and Emilien Girot from SAMPL-LRGP (Université de Lorraine-CNRS — https://lrgp-nancy.cnrs.fr/) and Alfonso Enrique Suarez for the informatic support.

CRediT authorship contribution statement

Catalina Suescun Gonzalez: Methodology, Experimentation, Data curation, Writing –original draft preparation.

Benjamin Sandei: Data curation, Writing – review & editing.

Fabio Cruz: Writing – review & editing.

Sandrine Hoppe: Validation, Writing – review & editing.

Joshua Pearce, Hakim Boudaoud, Cécile Nouvel: Supervision, Validation, Methodology, Writing – review & editing.

Data Availability Statement:

The data supporting the findings of this study are available from the authors upon request.

References

[1] J. Maris, S. Bourdon, J.-M. Brossard, L. Cauret, L. Fontaine, and V. Montembault, "Mechanical recycling: Compatibilization of mixed thermoplastic wastes," *Polymer Degradation and Stability*, vol. 147, pp. 245–266, Jan. 2018, doi: 10.1016/j.polymdegradstab.2017.11.001.

[2] Safwan-Ul-Iman, S. Rahman, M. Z. Rahman, B. Saha, and Z. Salsabil, "13.07 - Recent development trends on polymeric materials—Investigation of properties and applications," in *Comprehensive Materials Processing (Second Edition)*, S. Hashmi, Ed., Oxford: Elsevier, 2024, pp. 125–152. doi: 10.1016/B978-0-323-96020-5.00145-X.

[3] N. N. Fomina and V. G. Khozhin, "Compatibilization of polymer mixtures during processing of waste products from thermoplastics," *Nanobuild*, vol. 13, no. 4, pp. 229–236, Aug. 2021, doi: 10.15828/2075-8545-2021-13-4-229-236.

[4] J. Balwada, S. Samaiya, and R. P. Mishra, "Packaging Plastic Waste Management for a Circular Economy and Identifying a better Waste Collection System using Analytical Hierarchy Process (AHP)," *Procedia CIRP*, vol. 98, pp. 270–275, Jan. 2021, doi: 10.1016/j.procir.2021.01.102.

[5] R. Geyer, "Chapter 2 - Production, use, and fate of synthetic polymers," in *Plastic Waste and Recycling*, T. M. Letcher, Ed., Academic Press, 2020, pp. 13–32. doi: 10.1016/B978-0-12-817880-5.00002-5.

[6] P. Europe, "Plastics - the Facts 2019 • Plastics Europe," Plastics Europe. Accessed: Sep. 15, 2024. [Online]. Available: https://plasticseurope.org/knowledge-hub/plastics-the-facts-2019/

[7] N. Singh, D. Hui, R. Singh, I. P. S. Ahuja, L. Feo, and F. Fraternali, "Recycling of plastic solid waste: A state of art review and future applications," *Composites Part B: Engineering*, vol. 115, pp. 409–422, Apr. 2017, doi: 10.1016/j.compositesb.2016.09.013.

[8] A. Kassab, D. Al Nabhani, P. Mohanty, C. Pannier, and G. Y. Ayoub, "Advancing Plastic Recycling: Challenges and Opportunities in the Integration of 3D Printing and Distributed Recycling for a Circular Economy," *Polymers*, vol. 15, no. 19, Art. no. 19, Jan. 2023, doi: 10.3390/polym15193881.

[9] A. Ghosh, "Performance modifying techniques for recycled thermoplastics," *Resources, Conservation and Recycling*, vol. 175, p. 105887, Dec. 2021, doi: 10.1016/j.resconrec.2021.105887.

[10] S. Mbarek, M. Jaziri, Y. Chalamet, B. Elleuch, and C. Carrot, "Dispersed phase morphology and fractionated crystallization of high-density polyethylene in PET/HDPE blends," *International Journal of Material Forming*, vol. 2, no. 1, pp. 15–24, 2009, doi: 10.1007/s12289-008-0386-4.

[11] E. Parlament, "Directive (EU) 2019/904 of the European Parliament and of the Council of 5 June 2019 on the reduction of the impact of certain plastic products on the environment (Text with

EEA relevance)," https://webarchive.nationalarchives.gov.uk/eu-exit/https://eur-lex.europa.eu/legal-content/EN/TXT/?uri=CELEX:32019L0904. Accessed: Sep. 13, 2024. [Online]. Available: https://www.legislation.gov.uk/eudr/2019/904

[12] M. Nechifor, F. Tanasă, C.-A. Teacă, and M. Zănoagă, "Compatibilization strategies toward new polymer materials from re-/up-cycled plastics," *International Journal of Polymer Analysis and Characterization*, vol. 23, no. 8, pp. 740–757, Jan. 2018, doi: 10.1080/1023666X.2018.1509493.

[13] S. Bertin and J.-J. Robin, "Study and characterization of virgin and recycled LDPE/PP blends," *European Polymer Journal*, vol. 38, no. 11, pp. 2255–2264, Nov. 2002, doi: 10.1016/S0014-3057(02)00111-8.

[14] C. Fang, L. Nie, S. Liu, R. Yu, N. An, and S. Li, "Characterization of polypropylene–polyethylene blends made of waste materials with compatibilizer and nano-filler," *Composites Part B: Engineering*, vol. 55, pp. 498–505, Dec. 2013, doi: 10.1016/j.compositesb.2013.06.046.

[15] A. A. Yousefi, A. Ait-Kadi, and C. Roy, "Effect of elastomeric and plastomeric toughenersons different properties of recycled polyethylene," *Advances in Polymer Technology*, vol. 17, no. 2, pp. 127–143, 1998, doi: 10.1002/(SICI)1098-2329(199822)17:2<127::AID-ADV4>3.0.CO;2-V.

[16] I. Fortelný, D. Michálková, and Z. Kruliš, "An efficient method of material recycling of municipal plastic waste," *Polymer Degradation and Stability*, vol. 85, no. 3, pp. 975–979, Sep. 2004, doi: 10.1016/j.polymdegradstab.2004.01.024.

[17] P. K. S. Mural, S. Mohanty, S. K. Nayak, and S. Anbudayanidhi, "Polypropylene/high impact polystyrene blend nanocomposites obtained from E-waste: evaluation of mechanical, thermal and morphological properties," *Int J Plast Technol*, vol. 15, no. 1, pp. 46–60, Jan. 2011, doi: 10.1007/s12588-011-9005-1.

[18] R. M. C. Santana and S. Manrich, "Studies on morphology and mechanical properties of PP/HIPS blends from postconsumer plastic waste," *Journal of Applied Polymer Science*, vol. 87, no. 5, pp. 747–751, 2003, doi: 10.1002/app.11404.

[19] C. G. Iñiguez, E. Michel, V. M. González-Romero, and R. González-Nuñez, "Morphological stability of postconsumer PET/HDPE blends," *Polymer Bulletin*, vol. 45, no. 3, pp. 295–302, Nov. 2000, doi: 10.1007/s002890070034.

[20] Y. Zhang, H. Zhang, Y. Yu, W. Guo, and C. Wu, "Recycled poly(ethylene terephthalate)/linear low-density polyethylene blends through physical processing," *Journal of Applied Polymer Science*, vol. 114, no. 2, pp. 1187–1194, 2009, doi: 10.1002/app.30030.

[21] H. Zhang, W. Guo, Y. Yu, B. Li, and C. Wu, "Structure and properties of compatibilized recycled poly(ethylene terephthalate)/linear low density polyethylene blends," *European Polymer Journal*, vol. 43, no. 8, pp. 3662–3670, Aug. 2007, doi: 10.1016/j.eurpolymj.2007.05.001.

[22] H. Inoya, Y. Wei Leong, W. Klinklai, Y. Takai, and H. Hamada, "Compatibilization of recycled poly(ethylene terephthalate) and polypropylene blends: Effect of compatibilization on blend toughness, dispersion of minor phase, and thermal stability," *Journal of Applied Polymer Science*, vol. 124, no. 6, pp. 5260–5269, 2012, doi: 10.1002/app.34385.

[23] A. Farzadfar, S. N. Khorasani, and S. Khalili, "Blends of recycled polycarbonate and acrylonitrile–butadiene–styrene: comparing the effect of reactive compatibilizers on mechanical and morphological properties," *Polymer International*, vol. 63, no. 1, pp. 145–150, 2014, doi: 10.1002/pi.4493.

[24] S. M. Hong, S. S. Hwang, J. S. Choi, and H. J. Choi, "Compatibility effect of reactive copolymers on polypropylene/polyamide 6 blends from commingled plastic wastes," *Journal of Applied Polymer Science*, vol. 101, no. 2, pp. 1188–1193, 2006, doi: 10.1002/app.24075.

[25] N. Miskolczi, P. Kucharczyk, V. Sedlarik, and H. Szakacs, "Plastic waste minimization: Compatibilization of polypropylene/polyamide 6 blends by polyalkenyl-poly-maleic-anhydride-based agents," *Journal of Applied Polymer Science*, vol. 129, no. 5, pp. 3028–3037, 2013, doi: 10.1002/app.38724.

[26] G. H. Kim, S. S. Hwang, B. G. Cho, and S. M. Hong, "Reactive Extrusion of Polypropylene and Nylon Blends from Commingled Plastic Wastes," *Macromolecular Symposia*, vol. 249–250, no. 1, pp. 485–492, 2007, doi: 10.1002/masy.200750424.

[27] A. A. S. M. Atiqah, H. Salmah, Z. Firuz, and D. N. U. Lan, “Properties of Recycled High Density Polyethylene/Recycled Polypropylene Blends: Effect of Maleic Anhydride Polypropylene,” *Key Engineering Materials*, vol. 594–595, pp. 837–841, 2014, doi: 10.4028/www.scientific.net/KEM.594-595.837.
[28] A. A. S. M. Atiqah, H. Salmah, Z. Firuz, and D. n. u. Lan, “Effect of Different Blend Ratios and Compatibilizer on Tensile Properties of Recycled Poly(propylene)/Recycled High Density Polyethylene Blends,” *Macromolecular Symposia*, vol. 353, no. 1, pp. 70–76, 2015, doi: 10.1002/masy.201550309.
[29] Y. Lei, Q. Wu, C. M. Clemons, and W. Guo, “Phase structure and properties of poly(ethylene terephthalate)/high-density polyethylene based on recycled materials,” *J. Appl. Polym. Sci.*, vol. 113, no. 3, pp. 1710–1719, Aug. 2009, doi: 10.1002/app.30178.
[30] N. E. Zander, “Recycled Polymer Feedstocks for Material Extrusion Additive Manufacturing,” in *ACS Symposium Series*, vol. 1315, J. E. Seppala, A. P. Kotula, and C. R. Snyder, Eds., Washington, DC: American Chemical Society, 2019, pp. 37–51. doi: 10.1021/bk-2019-1315.ch003.
[31] H. Shahrajabian and F. Sadeghian, “The investigation of alumina nanoparticles’ effects on the mechanical and thermal properties of HDPE/rPET/MAPE blends,” *Int Nano Lett*, vol. 9, no. 3, pp. 213–219, Sep. 2019, doi: 10.1007/s40089-019-0273-7.
[32] L. Zhidan, S. Juncai, C. Chao, and Z. Xiuju, “Polypropylene/wasted poly(ethylene terephthalate) fabric composites compatibilized by two different methods: Crystallization and melting behavior, crystallization morphology, and kinetics,” *Journal of Applied Polymer Science*, vol. 121, no. 4, pp. 1972–1981, 2011, doi: 10.1002/app.33757.
[33] A. Hellati, D. Benachour, M. E. Cagiao, S. Boufassa, and F. J. Baltá Calleja, “Role of a compatibilizer in the structure and micromechanical properties of recycled poly(ethylene terephthalate)/polyolefin blends with clay,” *Journal of Applied Polymer Science*, vol. 118, no. 3, pp. 1278–1287, 2010, doi: 10.1002/app.32090.
[34] E. M. Akshaya, R. Palaniappan, C. F. Sowmya, N. Rasana, and K. Jayanarayanan, “Properties of Blends from Polypropylene and Recycled Polyethylene Terephthalate using a Compatibilizer,” *Materials Today: Proceedings*, vol. 24, pp. 359–368, Jan. 2020, doi: 10.1016/j.matpr.2020.04.287.
[35] R. M. Santos *et al.*, “Thermal and Rheological Characterization of Recycled PET/Virgin HDPE Blend Compatibilized with PE-g-MA and an Epoxy Chain Extender,” *Polymers*, vol. 14, no. 6, Art. no. 6, Jan. 2022, doi: 10.3390/polym14061144.
[36] M. N. Salleh, S. Ahmad, M. H. A. Ghani, and R. S. Chen, “Effect of compatibilizer on impact and morphological analysis of recycled HDPE/PET blends,” presented at the THE 2013 UKM FST POSTGRADUATE COLLOQUIUM: Proceedings of the Universiti Kebangsaan Malaysia, Faculty of Science and Technology 2013 Postgraduate Colloquium, Selangor, Malaysia, 2013, pp. 70–74. doi: 10.1063/1.4858632.
[37] M. K. Akkapeddi, B. Van Buskirk, C. D. Mason, S. S. Chung, and X. Swamikannu, “Performance blends based on recycled polymers,” *Polymer Engineering & Science*, vol. 35, no. 1, pp. 72–78, 1995, doi: 10.1002/pen.760350110.
[38] A. S. Adekunle, A. A. Adeleke, C. V. Sam Obu, P. P. Ikubanni, S. E. Ibitoye, and T. M. Azeez, “Recycling of plastics with compatibilizer as raw materials for the production of automobile bumper,” *Cogent Engineering*, vol. 7, no. 1, p. 1801247, Jan. 2020, doi: 10.1080/23311916.2020.1801247.
[39] R. S. Chen, S. Ahmad, M. H. A. Ghani, and M. N. Salleh, “Optimization of high filler loading on tensile properties of recycled HDPE/PET blends filled with rice husk,” presented at the THE 2014 UKM FST POSTGRADUATE COLLOQUIUM: Proceedings of the Universiti Kebangsaan Malaysia, Faculty of Science and Technology 2014 Postgraduate Colloquium, Selangor, Malaysia, 2014, pp. 46–51. doi: 10.1063/1.4895168.
[40] M. Pluta, Z. Bartczak, A. Pawlak, A. Galeski, and M. Pracella, “Phase structure and viscoelastic properties of compatibilized blends of PET and HDPE recyclates,” *Journal of Applied Polymer Science*, vol. 82, no. 6, pp. 1423–1436, 2001, doi: 10.1002/app.1980.

[41] U. Habib, Z. I. Khan, and Z. B. Mohamad, “Compatibility and miscibility of recycled polyethylene terephthalate/polyamide 11 blends with and without Joncryl® compatibilizer: a comprehensive study of mechanical, thermal, and thermomechanical properties,” *Iran Polym J*, vol. 33, no. 9, pp. 1313–1326, Sep. 2024, doi: 10.1007/s13726-024-01357-y.
[42] Z. I. Khan *et al.*, “Enhanced Mechanical and Thermal Performance of Sustainable RPET/PA-11/Joncryl® Nanocomposites Reinforced with Halloysite Nanotubes,” *Polymers*, vol. 17, no. 11, p. 1433, Jan. 2025, doi: 10.3390/polym17111433.
[43] N. Othman, Z. Mohamad, Z. I. Khan, and L. C. Abdullah, “Rheological behavior of recycled poly(ethylene terephthalate) /poly(amide) 11 blends with chain extender,” *Materials Today: Proceedings*, vol. 110, pp. 87–90, Jan. 2024, doi: 10.1016/j.matpr.2023.09.097.
[44] Y. Zhu, C. Liang, Y. Bo, and S. Xu, “Non-isothermal crystallization behavior of compatibilized polypropylene/recycled polyethylene terephthalate blends,” *J Therm Anal Calorim*, vol. 119, no. 3, pp. 2005–2013, Mar. 2015, doi: 10.1007/s10973-014-4349-3.
[45] Z. O. Oyman and T. Tinçer, “Melt blending of poly(ethylene terephthalate) with polypropylene in the presence of silane coupling agent,” *Journal of Applied Polymer Science*, vol. 89, no. 4, pp. 1039–1048, 2003, doi: 10.1002/app.12228.
[46] S. Razavi, A. Shojaei, and R. Bagheri, “Binary and ternary blends of high-density polyethylene with poly(ethylene terephthalate) and polystyrene based on recycled materials,” *Polymers for Advanced Technologies*, vol. 22, no. 5, pp. 690–702, 2011, doi: 10.1002/pat.1567.
[47] S. Kayaisang, T. Amornsakchai, and S. Saikrasun, “Influence of liquid crystalline polymer and recycled PET as minor blending components on rheological behavior, morphology, and thermal properties of thermoplastic blends,” *Polymers for Advanced Technologies*, vol. 20, no. 12, pp. 1136–1145, 2009, doi: 10.1002/pat.1389.
[48] F. A. Cruz Sanchez, H. Boudaoud, M. Camargo, and J. M. Pearce, “Plastic recycling in additive manufacturing: A systematic literature review and opportunities for the circular economy,” *Journal of Cleaner Production*, vol. 264, p. 121602, Aug. 2020, doi: 10.1016/j.jclepro.2020.121602.
[49] S. C. Dertinger *et al.*, “Technical pathways for distributed recycling of polymer composites for distributed manufacturing: Windshield wiper blades,” *Resources, Conservation and Recycling*, vol. 157, p. 104810, Jun. 2020, doi: 10.1016/j.resconrec.2020.104810.
[50] M. Mohammed, D. Wilson, E. Gomez-Kervin, A. Petsiuk, R. Dick, and J. M. Pearce, “Sustainability and feasibility assessment of distributed E-waste recycling using additive manufacturing in a Bi-continental context,” *Additive Manufacturing*, vol. 50, p. 102548, Feb. 2022, doi: 10.1016/j.addma.2021.102548.
[51] H. A. Little, N. G. Tanikella, M. J. Reich, M. J. Fiedler, S. L. Snabes, and J. M. Pearce, “Towards Distributed Recycling with Additive Manufacturing of PET Flake Feedstocks,” *Materials*, vol. 13, no. 19, Art. no. 19, Jan. 2020, doi: 10.3390/ma13194273.
[52] J. M. J. Netto *et al.*, “DESIGN AND VALIDATION OF AN INNOVATIVE 3D PRINTER CONTAINING A CO-ROTATING TWIN SCREW EXTRUSION UNIT,” *Additive Manufacturing*, p. 103192, Oct. 2022, doi: 10.1016/j.addma.2022.103192.
[53] A. Romani, M. Levi, and J. M. Pearce, “Recycled Polycarbonate and Polycarbonate/Acrylonitrile Butadiene Styrene Feedstocks for Circular Economy Product Applications with Fused Granular Fabrication-Based Additive Manufacturing,” Jul. 12, 2023, *Rochester, NY*: 4508039. doi: 10.2139/ssrn.4508039.
[54] J. Domingues, T. Marques, A. Mateus, P. Carreira, and C. Malça, “An Additive Manufacturing Solution to Produce Big Green Parts from Tires and Recycled Plastics,” *Procedia Manufacturing*, vol. 12, pp. 242–248, Jan. 2017, doi: 10.1016/j.promfg.2017.08.028.
[55] Amanda, “Kraton G Hydrogenated Styrenic Block Copolymers | Kraton.” Accessed: Dec. 23, 2024. [Online]. Available: https://kraton.com/products/kraton-g/
[56] C. Suescun Gonzalez, F. A. Cruz Sanchez, H. Boudaoud, C. Nouvel, and J. M. Pearce, “Multi-material distributed recycling via material extrusion: recycled high density polyethylene and

poly (ethylene terephthalate) mixture," *Polymer Engineering & Science*, vol. n/a, no. n/a, 2024, doi: 10.1002/pen.26643.
[57] S. K. Taghavi, H. Shahrajabian, and H. M. Hosseini, "Detailed comparison of compatibilizers MAPE and SEBS-g-MA on the mechanical/thermal properties, and morphology in ternary blend of recycled PET/HDPE/MAPE and recycled PET/HDPE/SEBS-g-MA," *Journal of Elastomers & Plastics*, vol. 50, no. 1, pp. 13–35, Feb. 2018, doi: 10.1177/0095244317698738.
[58] A. L. Woern, D. J. Byard, R. B. Oakley, M. J. Fiedler, S. L. Snabes, and J. M. Pearce, "Fused Particle Fabrication 3-D Printing: Recycled Materials' Optimization and Mechanical Properties," *Materials*, vol. 11, no. 8, Art. no. 8, Aug. 2018, doi: 10.3390/ma11081413.
[59] Z. Chen, J. N. Hay, and M. J. Jenkins, "FTIR spectroscopic analysis of poly(ethylene terephthalate) on crystallization," *European Polymer Journal*, vol. 48, no. 9, pp. 1586–1610, Sep. 2012, doi: 10.1016/j.eurpolymj.2012.06.006.
[60] Y. Pan, G. Wu, H. Ma, S. Zhou, and H. Zhang, "Improved compatibility of PET/HDPE blend by using GMA grafted thermoplastic elastomer," *Polymer-Plastics Technology and Materials*, vol. 59, no. 17, pp. 1887–1898, Nov. 2020, doi: 10.1080/25740881.2020.1765382.
[61] S. Kim, C. E. Park, J. H. An, D. Lee, and J. Kim, "The Effect of Functional Group Content on Poly(ethylene terephthalate)/High Density Polyethylene Blends Compatibilized with Poly(ethylene-co-acrylic acid)," *Polym J*, vol. 29, no. 3, Art. no. 3, Mar. 1997, doi: 10.1295/polymj.29.274.
[62] V. A. Escócio, E. B. A. V. Pacheco, A. L. N. da Silva, A. de P. Cavalcante, and L. L. Y. Visconte, "Rheological Behavior of Renewable Polyethylene (HDPE) Composites and Sponge Gourd (*Luffa cylindrica*) Residue," *International Journal of Polymer Science*, vol. 2015, pp. 1–7, 2015, doi: 10.1155/2015/714352.
[63] "Standard Test Method for Melt Flow Rates of Thermoplastics by Extrusion Plastometer." Accessed: Nov. 18, 2025. [Online]. Available: https://store.astm.org/d1238-10.html
[64] "ISO 527-1:2019," ISO. Accessed: Apr. 05, 2025. [Online]. Available: https://www.iso.org/standard/75824.html
[65] "ISO 179-1:2023," ISO. Accessed: Nov. 18, 2025. [Online]. Available: https://www.iso.org/fr/standard/84393.html
[66] F. Kučera, J. Petruš, J. Žídek, P. Poláček, and M. Šimonek, "An approach on reactive processing of plastic waste," *Polymer Engineering & Science*, vol. 62, no. 12, pp. 4100–4114, 2022, doi: 10.1002/pen.26170.
[67] Y. Mao, W. Cao, Q. Li, and C. Wu, "Study of 'one-step' preparation of r-PET fiber-reinforced PE composites," *Mater. Res. Express*, vol. 8, no. 8, p. 085302, Aug. 2021, doi: 10.1088/2053-1591/ac1aa7.
[68] D. Grime and I. M. Ward, "The assignment of infra-red absorptions and rotational isomerism in polyethylene terephthalate and related compounds," *Trans. Faraday Soc.*, vol. 54, no. 0, pp. 959–971, Jan. 1958, doi: 10.1039/TF9585400959.
[69] W. H. Cobbs Jr. and R. L. Burton, "Crystallization of polyethylene terephthalate," *Journal of Polymer Science*, vol. 10, no. 3, pp. 275–290, 1953, doi: 10.1002/pol.1953.120100302.
[70] F. P. L. Mantia, M. Ceraulo, G. Giacchi, M. C. Mistretta, and L. Botta, "Effect of a Compatibilizer on the Morphology and Properties of Polypropylene/Polyethylentherephthalate Spun Fibers," *Polymers*, vol. 9, no. 2, Art. no. 2, Feb. 2017, doi: 10.3390/polym9020047.
[71] J. E. K. Schawe, "An analysis of the meta stable structure of poly(ethylene terephthalate) by conventional DSC," *Thermochimica Acta*, vol. 461, no. 1, pp. 145–152, Sep. 2007, doi: 10.1016/j.tca.2007.05.017.
[72] R. Brandalise, R. Mauler, and M. Zeni, "BLENDS OF HIGH DENSITY POLYETHYLENE AND POLY (ETHYLENE TEREPHTHALATE)," Mar. 2022.
[73] Y. Kong and J. N. Hay, "Multiple melting behaviour of poly(ethylene terephthalate)," *Polymer*, vol. 44, no. 3, pp. 623–633, Jan. 2003, doi: 10.1016/S0032-3861(02)00814-5.

[74] M. A. S. Spinacé and M. A. De Paoli, “Characterization of poly(ethylene terephtalate) after multiple processing cycles,” *Journal of Applied Polymer Science*, vol. 80, no. 1, pp. 20–25, 2001, doi: 10.1002/1097-4628(20010404)80:1<20::AID-APP1069>3.0.CO;2-S.
[75] I. A. M. Al Raheil, “Morphology and crystallization of poly(ethylene terephthalate),” *Polymer International*, vol. 35, no. 2, pp. 189–195, 1994, doi: 10.1002/pi.1994.210350209.
[76] X. Lin *et al.*, “Melt rheology and properties of compatibilized recycled poly(ethylene terephthalate)/(styrene-ethylene-ethylene-propylene-styrene) block copolymer blends,” *Journal of Vinyl and Additive Technology*, vol. 22, no. 3, pp. 342–349, 2016, doi: 10.1002/vnl.21450.
[77] D. Acierno and A. Patti, “Fused Deposition Modelling (FDM) of Thermoplastic-Based Filaments: Process and Rheological Properties—An Overview,” *Materials*, vol. 16, no. 24, Art. no. 24, Jan. 2023, doi: 10.3390/ma16247664.
[78] H. Staudinger and W. Heuer, “Über hochpolymere Verbindungen, 33. Mitteilung: Beziehungen zwischen Viscosität und Molekulargewicht bei Poly-styrolen,” *Berichte der deutschen chemischen Gesellschaft (A and B Series)*, vol. 63, no. 1, pp. 222–234, 1930, doi: 10.1002/cber.19300630129.
[79] C.-H. Jiang, G.-J. Zhong, and Z.-M. Li, “Recyclability of In Situ Microfibrillar Poly(ethylene terephthalate)/High-Density Polyethylene Blends,” *Macromolecular Materials and Engineering*, vol. 292, no. 3, pp. 362–372, 2007, doi: 10.1002/mame.200600356.
[80] L. A. Pinheiro, M. A. Chinelatto, and S. V. Canevarolo, “The role of chain scission and chain branching in high density polyethylene during thermo-mechanical degradation,” *Polymer Degradation and Stability*, vol. 86, no. 3, pp. 445–453, Dec. 2004, doi: 10.1016/j.polymdegradstab.2004.05.016.
[81] P. Oblak, J. Gonzalez-Gutierrez, B. Zupančič, A. Aulova, and I. Emri, “Processability and mechanical properties of extensively recycled high density polyethylene,” *Polymer Degradation and Stability*, vol. 114, pp. 133–145, Apr. 2015, doi: 10.1016/j.polymdegradstab.2015.01.012.
[82] T. Kealy, “Rheological analysis of the degradation of HDPE during consecutive processing steps and for different processing conditions,” *Journal of Applied Polymer Science*, vol. 112, no. 2, pp. 639–648, 2009, doi: 10.1002/app.29418.
[83] M. Garwacki, I. Cudnik, D. Dziadowiec, P. Szymczak, and J. Andrzejewski, “The Development of Sustainable Polyethylene Terephthalate Glycol-Based (PETG) Blends for Additive Manufacturing Processing—The Use of Multilayered Foil Waste as the Blend Component,” *Materials*, vol. 17, no. 5, Art. no. 5, Jan. 2024, doi: 10.3390/ma17051083.
[84] K. Formela and B. Eyigöz, “Planetary roller extruders in the sustainable development of polymer blends and composites – Past, present and future. | Express Polymer Letters | EBSCOhost.” Accessed: May 05, 2024. [Online]. Available: https://openurl.ebsco.com/contentitem/doi:10.3144%2Fexpresspolymlett.2024.32?sid=ebsco:plink:crawler&id=ebsco:doi:10.3144%2Fexpresspolymlett.2024.32
[85] I. Fortelný, M. Lapčíková, F. Lednický, Z. Starý, and Z. Kruliš, “Non-uniform phase structure in immiscible polymer blends - reasons and consequences,” *Polimery*, vol. 54, no. 2, Art. no. 2, Feb. 2009.
[86] G. Graninger, S. Kumar, G. Garrett, and B. G. Falzon, “Effect of shear forces on dispersion-related properties of microcrystalline cellulose-reinforced EVOH composites for advanced applications,” *Composites Part A: Applied Science and Manufacturing*, vol. 139, p. 106103, Dec. 2020, doi: 10.1016/j.compositesa.2020.106103.
[87] Z. Kordjazi and N. G. Ebrahimi, “Rheological behavior of noncompatibilized and compatibilized PP/PET blends with SEBS-g-MA,” *Journal of Applied Polymer Science*, vol. 116, no. 1, pp. 441–448, 2010, doi: 10.1002/app.31471.
[88] J. Gao, G. C. Walsh, D. Bigio, R. M. Briber, and M. D. Wetzel, “Residence-time distribution model for twin-screw extruders,” *AIChE Journal*, vol. 45, no. 12, pp. 2541–2549, 1999, doi: 10.1002/aic.690451210.

[89] R. Navarro, F. Parres, J. E. Crespo, S. Sánchez-Caballero, and M. A. Sellés, “COMPATIBILIZATION OF POSTCONSUMER PET/HDPE BLENDS.,” p. 2, 2020.
[90] T. D. Traugott, J. W. Barlow, and D. R. Paul, “Mechanical compatibilization of high density polyethylene–poly(ethylene terephthalate) blends,” *Journal of Applied Polymer Science*, vol. 28, no. 9, pp. 2947–2959, 1983, doi: 10.1002/app.1983.070280922.
[91] K. Dobrovszky and F. Ronkay, “Effects of SEBS-g-MA on rheology, morphology and mechanical properties of PET/HDPE blends”, doi: DOI: 10.3139/217.2970.
[92] H. Inoya, Y. Wei Leong, W. Klinklai, S. Thumsorn, Y. Makata, and H. Hamada, “Compatibilization of recycled poly(ethylene terephthalate) and polypropylene blends: Effect of polypropylene molecular weight on homogeneity and compatibility,” *Journal of Applied Polymer Science*, vol. 124, no. 5, pp. 3947–3955, 2012, doi: 10.1002/app.34405.
[93] M. Quaresimin, K. Schulte, M. Zappalorto, and S. Chandrasekaran, “Toughening mechanisms in polymer nanocomposites: From experiments to modelling,” *Composites Science and Technology*, vol. 123, pp. 187–204, Feb. 2016, doi: 10.1016/j.compscitech.2015.11.027.
[94] W. H. Lee, “Toughened polymers,” in *Polymer Blends and Alloys*, M. J. Folkes and P. S. Hope, Eds., Dordrecht: Springer Netherlands, 1993, pp. 163–194. doi: 10.1007/978-94-011-2162-0_7.
[95] A. S. Argon, R. E. Cohen, and T. M. Mower, “Mechanisms of toughening brittle polymers,” *Materials Science and Engineering: A*, vol. 176, no. 1, pp. 79–90, Mar. 1994, doi: 10.1016/0921-5093(94)90961-X.
[96] S. Sánchez-Valdes, L. F. Ramos-De Valle, and O. Manero, “Polymer Blends,” in *Handbook of Polymer Synthesis, Characterization, and Processing*, John Wiley & Sons, Ltd, 2013, pp. 505–517. doi: 10.1002/9781118480793.ch27.
[97] H. Ismail H. and M. Nasir, “The effect of various compatibilizers on mechanical properties of polystyrene/polypropylene blend,” *Polymer Testing*, vol. 21, no. 2, pp. 163–170, Jan. 2002, doi: 10.1016/S0142-9418(01)00064-2.
[98] B. Wittbrodt and J. M. Pearce, “The effects of PLA color on material properties of 3-D printed components,” *Additive Manufacturing*, vol. 8, pp. 110–116, Oct. 2015, doi: 10.1016/j.addma.2015.09.006.
[99] J. Kasama, “Compatibilization of recycled high density polyethylene (HDPE)/polyethylene terephthalate (PET) blends,” 2007. Accessed: Sep. 15, 2024. [Online]. Available: https://www.semanticscholar.org/paper/Compatibilization-of-recycled-high-density-%28HDPE%29-Kasama/ef1ec001aa78d3b3b2abe8d755b3a5489b72726e